Catalysis Today xxx (xxxx) xxx



Contents lists available at ScienceDirect

## Catalysis Today

journal homepage: www.elsevier.com/locate/cattod



## Molecular structure and catalytic promotional effect of Mn on supported Na<sub>2</sub>WO<sub>4</sub>/SiO<sub>2</sub> catalysts for oxidative coupling of methane (OCM) reaction

Sagar Sourav $^{a,b,1}$ , Daniyal Kiani $^{a,2}$ , Yixiao Wang $^{b,*,3}$ , Jonas Baltrusaitis $^{a,*,4}$ , Rebecca R. Fushimi $^{b,*,5}$ , Israel E. Wachs $^{a,*,6}$ 

### ARTICLE INFO

### Keywords: OCM Mn-Na2WO4/SiO2 catalyst Active site In-situ spectroscopy In-situ Raman TAP Kinetics Mn promotional effect

### ABSTRACT

The structure and promotional effect of Mn in supported Mn-Na<sub>2</sub>WO<sub>4</sub>/SiO<sub>2</sub> catalysts for the oxidative coupling of methane (OCM) reaction has been debated for a longtime in the literature. In the current investigation, with the aid of multiple in-situ characterization studies, we show that the freshly calcined supported 1.2Mn-5Na<sub>2</sub>WO<sub>4</sub>/ SiO<sub>2</sub> catalyst possesses crystalline Na<sub>2</sub>WO<sub>4</sub>, Mn<sub>2</sub>O<sub>3</sub> and SiO<sub>2</sub> (cristobalite phase) along with surface MnO<sub>x</sub> and Na-WO<sub>x</sub> sites at low temperature and oxidizing environments. Under the OCM reaction environment (T > 800  $^{\circ}$ C), the crystalline Na<sub>2</sub>WO<sub>4</sub> phase melts and Mn<sub>2</sub>O<sub>3</sub> phase reduces. In contrast, the surface MnO<sub>x</sub> and Na- $WO_x$  sites exhibit excellent thermal and chemical stability. Exposure of the 1.2Mn-5Na<sub>2</sub>WO<sub>4</sub>/SiO<sub>2</sub> catalyst to the OCM reaction environment redisperses the molten Na<sub>2</sub>WO<sub>4</sub> phase on the SiO<sub>2</sub> support to form new surface WO<sub>x</sub> sites. Interestingly, the stable MnOx species interacts with both molten Na2WO4 phase and surface Na-WOx sites during OCM reaction. Controlled transient kinetic experiments in TAP and detailed steady state OCM fixed-bed reaction studies reveal the role and promotional effect of Mn in the 1.2Mn-5Na<sub>2</sub>WO<sub>4</sub>/SiO<sub>2</sub> catalyst. The W-oxides (both molten Na<sub>2</sub>WO<sub>4</sub> and surface Na-WO<sub>x</sub> sites) are the active sites for the catalytic OCM reaction and the MnO<sub>x</sub> species only function as promoters. The promotion of MnOx strongly depends on the gas phase O2 partial pressure and the MnOx species act as mediators for oxygen exchange between the gas phase molecular O2 and catalyst lattice oxygen. The temperature dependent MnOx promotion reveals that the MnOx species selectively promote the molten Na<sub>2</sub>WO<sub>4</sub> phase at lower reaction temperature and the surface Na-WO<sub>x</sub> sites at higher temperature.

### 1. Introduction

The oxidative coupling of methane (OCM) is a single-step process for the conversion of CH<sub>4</sub>, the major component of natural gas, to valueadded C2 products (C2H6 and C2H4). Among the many catalysts tested for this reaction, the Na-promoted SiO<sub>2</sub> supported W-oxide based catalysts have been found very active, selective and stable for extended operation. [1,2] The addition of MnOx to supported Na2WO4/SiO2 catalysts significantly improves the catalytic OCM performance. [3-6] This has led to extensive investigations in the literature to understand the structure and promotion mechanism(s) of MnOx.

The early studies on the structure of supported Mn-Na<sub>2</sub>WO<sub>4</sub>/SiO<sub>2</sub> catalysts employed only characterization studies under ambient and/or ex-situ conditions that were unable to provide relevant information regarding the nature of the catalytic active sites during the OCM reaction. [5,6] Only recently, have in-situ/operando catalyst characterization studies been reported that are revealing the dynamic nature of the supported Mn-Na<sub>2</sub>WO<sub>4</sub>/SiO<sub>2</sub> catalysts as a function of environmental conditions. [7-18] Both XRD and Raman showed that the crystalline α-cristobalite phase of the SiO<sub>2</sub> support in freshly calcined catalyst

E-mail addresses: vixiao.wang@inl.gov (Y. Wang), job314@lehigh.edu (J. Baltrusaitis), rebecca.fushimi@inl.gov (R.R. Fushimi), jew0@lehigh.edu (I.E. Wachs).

### https://doi.org/10.1016/j.cattod.2022.07.005

Received 3 April 2022; Received in revised form 22 June 2022; Accepted 7 July 2022 Available online 13 July 2022

0920-5861/© 2022 Elsevier B.V. All rights reserved.

Please cite this article as: Sagar Sourav, Catalysis Today, https://doi.org/10.1016/j.cattod.2022.07.005

a Department of Chemical and Biomolecular Engineering, Lehigh University, Bethlehem, PA 18015, USA

b Catalysis and Transient Kinetics, Energy Environment Science & Technology, Idaho National Laboratory, Idaho Falls, ID 83415, USA

<sup>\*</sup> Corresponding authors.

 $<sup>^{1}</sup>$  0000–0001-5892–1329

<sup>2 0000-0002-9748-3007</sup> 

<sup>3 0000-0002-1446-3634</sup> 

<sup>&</sup>lt;sup>4</sup> 0000–0001-5634–955X

<sup>&</sup>lt;sup>5</sup> 0000–0002-7570–0234

 $<sup>^{6}</sup>$  0000–0001-5282–128X

transforms to crystalline the  $\beta$ -cristobalite phase at elevated temperatures (>  $\sim\!250~^\circ\text{C}$ ). [7–13,15–17] The SiO $_2$ -supported Na $_2$ WO $_4$  phase undergoes multiple phase transformations with temperature (crystalline cubic phase (<650  $^\circ\text{C}$ )  $\rightarrow$  crystalline orthorhombic phase (650–750  $^\circ\text{C}$ )  $\rightarrow$  molten amorphous phase (>750  $^\circ\text{C}$ )) as shown by XRD and Raman. [9,13,15,16] The presence of MnO $_x$  was found to increase the melting point of crystalline Na $_2$ WO $_4$  by  $\sim\!30~^\circ\text{C}$ . [16] Furthermore, in-situ Raman studies revealed that the molten Na $_2$ WO $_4$  phase is unstable at elevated temperatures (> 700  $^\circ\text{C}$ ) and transforms to surface Na-coordinated WO $_x$  (Na-WO $_x$ ) sites by dispersion on the SiO $_2$  support. [15] Additional studies showed that the surface Na-WO $_x$  sites are thermally stable and catalytically active for the OCM reaction [12,14,15].

Although a general consensus has been reached in the literature regarding the stable structures of the SiO2 support and Na-promoted WO<sub>x</sub> phases under OCM relevant conditions, there is still ongoing debate regarding the stable structure(s) of the MnO<sub>x</sub> phase. Only the crystalline Mn<sub>2</sub>O<sub>3</sub> phase was detected by XRD in oxidizing environments. [7,16] Complementary in-situ Raman studies also identified the crystalline  $\alpha$ -Mn<sub>2</sub>O<sub>3</sub>,  $\gamma$ -Mn<sub>2</sub>O<sub>3</sub>, and Mn<sup>2+</sup>Mn<sub>2</sub><sup>3+</sup>O<sub>4</sub> (hausmanite) phases as present in oxidizing environment (25-800 °C). [16] Subsequent in-situ XRD analysis under the OCM reaction environment observed a significant reduction in the intensity or even the absence of the crystalline Mn<sub>2</sub>O<sub>3</sub> phase [8,11] and it was speculated that the Mn-oxide phase is either reduced or present as an amorphous phase during the OCM reaction. [11] A few other studies, however, observed the formation of the crystalline MnWO<sub>4</sub> phase after melting of Na<sub>2</sub>WO<sub>4</sub> or under an OCM reaction environment with a high CH<sub>4</sub>/O<sub>2</sub> ratio. [9,10] The crystalline Mn<sub>7</sub>SiO<sub>12</sub> phase has also been reported to be present for supported Mn-Na<sub>2</sub>WO<sub>4</sub>/SiO<sub>2</sub> catalysts below ~650 °C. [13] At higher temperatures and OCM reaction environment, the crystalline Mn<sub>7</sub>SiO<sub>12</sub> phase was reported to disappear along with the melting of Na<sub>2</sub>WO<sub>4</sub> phase with concomitant appearance of the crystalline MnWO<sub>4</sub> phase. The lack of consensus in the literature regarding the stable structure of the MnOx phase warrants additional molecular level investigation via in-situ /operando spectroscopic characterization.

Different opinions are also seen in the litertaure regarding the role of the MnO<sub>x</sub> phase (catalytic active site for OCM vs. promoter) and its promotional effect on the W-oxide phases during the OCM reaction. In a few reports, the (distorted) WO<sub>4</sub> site present in the crystalline Na<sub>2</sub>WO<sub>4</sub> lattice was proposed to be the active site for the OCM reaction over supported Mn-Na<sub>2</sub>WO<sub>4</sub>/SiO<sub>2</sub> catalysts, and Mn-oxide was reported to participate in oxygen spillover to the W-oxide centers. [3,19–23] It was also reported that the bulk MnO4 and MnO6 oxide centers are responsible for both CH<sub>4</sub> and O<sub>2</sub> activation, respectively. [24] The second proposal regarding the role of Mn raises the question as to the role of the W-oxide phase for the OCM reaction. The oxygen in the bridging Na-O-Mn bond was also proposed as the active site because of the similar catalytic performances for Mn-Na<sub>2</sub>WO<sub>4</sub>/SiO<sub>2</sub>, Mn-Na<sub>2</sub>WO<sub>4</sub>/MgO and NaMnO<sub>4</sub>/MgO catalysts. [25] Both oxygen atoms on the bridging Na-O-Mn and Na-O-W were proposed as active sites in another study because of the substantial role of all three active metal oxides in the Mn-Na<sub>2</sub>WO<sub>4</sub>/SiO<sub>2</sub> catalyst system. [26] For the same reason, the interface between crystalline Mn<sub>2</sub>O<sub>3</sub> and Na<sub>2</sub>WO<sub>4</sub> phases was also speculated to be the active site. [27] The crystalline Mn<sub>2</sub>O<sub>3</sub> phase was also proposed to be an active site because of its excellent redox behavior. [7] Furthermore, a recent DFT study emphasized that surface Mn oxo sites present on the Mn<sub>2</sub>O<sub>3</sub> crystal as the active site for the CH<sub>4</sub> activation due to the higher energy barrier associated with the W oxo sites. [28] In contrast, oligomeric MnOx, Mn-WO3 and MnWO4 phases of Mn-oxides present in the supported Mn-Na-WO<sub>x</sub>/SiO<sub>2</sub> catalysts (with low Na loadings to avoid formation of crystalline Na<sub>2</sub>WO<sub>4</sub> phase) were not found to contribute towards the OCM reaction chemistry. [14] Additionally, the Mn-oxide has also been proposed to function as a promoter for the low temperature OCM reaction. [29] In summary, there is no consensus regarding the role and promotional effect of Mn-oxide towards the OCM reaction over supported Mn-Na<sub>2</sub>WO<sub>4</sub>/SiO<sub>2</sub>.

The involvement of lattice oxygen species in the supported Mn-Na<sub>2</sub>WO<sub>4</sub>/SiO<sub>2</sub> catalysts for CH<sub>4</sub> activation and oxidation is also considered paramount in the OCM literature. [13,17,30-34] These studies, however, did not undertake detailed investigation into the nature and origin of active lattice oxygen species and/or their roles in the OCM reaction network. [35] Recent in-situ spectroscopic and transient kinetic investigations showed that the supported Na<sub>2</sub>WO<sub>4</sub>/SiO<sub>2</sub> catalysts possess two different types of oxygen species: (i) atomic O species associated with the surface Na-WOx sites primarily responsible for formation of C2 products, and (ii) dioxygen O2 species originating from the molten Na<sub>2</sub>WO<sub>4</sub> phase involved in the production of CO<sub>2</sub> and oxidative dehydrogenation of C<sub>2</sub>H<sub>6</sub>. [15,35] The addition of MnO<sub>x</sub> to the supported Na<sub>2</sub>WO<sub>4</sub>/SiO<sub>2</sub> catalysts was shown to improve the total amount and release rate of O<sub>2</sub> species associated with the molten Na<sub>2</sub>WO<sub>4</sub> phase. Furthermore, the addition of MnO<sub>x</sub> was found to improve the C<sub>2</sub> product selectivity. [35] Despite these significant findings, several important points still need further clarification: (i) is the MnOx phase by itself active towards OCM? if so, then how selective is that activation step? (ii) does MnOx act as the active center or just play the role of promoter in supported Mn-Na<sub>2</sub>WO<sub>4</sub>/SiO<sub>2</sub> catalysts? (iii) how does the promotion effect of MnO<sub>x</sub> vary with reaction conditions (temperature, gas-space velocities, long-term catalyst stability, etc.)? (iv) how does MnO<sub>v</sub> change the reaction chemistry of the Na<sub>2</sub>WO<sub>4</sub>/SiO<sub>2</sub> catalyst?

The current investigation, with the aid of multiple *in-situ* characterization techniques (Raman spectroscopy, XRD, NAP-XPS (near ambient pressure X-ray photelectron spectroscopy)), aims at revealing the stable structure of the  $MnO_x$  phase in supported  $Mn-Na_2WO_4/SiO_2$  catalysts during the OCM reaction. Addionally, with the aid of  $H_2$ -TPR (temperature programmed reduction), controlled transient reaction studies in TAP (temporal analysis of products) and detailed steady state fixed-bed reactor kinetic studies, we aim at resolving the roles and promotional effect of  $MnO_x$  in supported  $Mn-Na_2WO_4/SiO_2$  catalysts towards the OCM reaction network.

### 2. Experimental

### 2.1. Catalyst Synthesis

The catalysts were synthesized using the incipient wetness impregnation (IWI) method. At first, the SiO<sub>2</sub> support (Cabot CAB-O-SIL® EH5) was treated with water and crushed into a fine powder (100-150  $\mu m$ particle size), as described previously. [15] The required amount of aqueous solution of Na2WO4•2H2O was impregnated into the water-treated SiO2 support, followed by overnight drying at room temperature. Subsequently, an aqueous Mn(NO<sub>3</sub>)<sub>2</sub>•xH<sub>2</sub>O solution of the required amount was impregnated into the above sample and was again dried overnight at room temperature. The above sample was further dried at 120 °C for 2 h, and finally calcined at 800 °C for 8 h, under flowing air. For the preparation of Na<sub>2</sub>WO<sub>4</sub>/SiO<sub>2</sub> and Mn/SiO<sub>2</sub> catalysts only the desired metal oxide precursor was incorporated into the SiO2 support, and the drying and calcination steps followed were similar to as described above. The catalysts were named according to the weight loadings of the active metal/metal-oxide components. For example, the supported 1.2Mn-5Na<sub>2</sub>WO<sub>4</sub>/SiO<sub>2</sub> catalyst contains 1.2 % of Mn and 5 % of Na<sub>2</sub>WO<sub>4</sub> on weight basis.

The powder sample (100–150  $\mu m$  particle size), as received after the calcination step is used for *in-situ* Raman and H<sub>2</sub>-TPR experiments. For *in-situ* XRD and NAP-XPS studies the powder sample was pressed to form a thin disk. For TAP and steady-state kinetic studies, the powder samples were pressed to form pellets and then crushed to obtain 250–300  $\mu m$  size particles.

### 2.2. In-situ XRD

The powder X-Ray diffraction (XRD) was recorded by a Bruker-AXS D5005 (Bruker, Billerica, MA, USA) with a Co  $K_{\alpha}$  source. For the

experiment, the sample was first pressed to form a disk, which was then mounted on a gold foil before placing it on the heater plate. Then the sample temperature was increased to 400 °C (at 10 °C/min), under constant flow ( $\sim$  50 cc/min) of dry air. After the dehydration of the sample at 400 °C for 1 h, the XRD spectrum was collected. Following that, the sample was heated to 900 °C (at 10 °C/min), in the same gas environment, and another spectrum was collected. Before the analysis of the XRD data, the signal from the gold foil was subtracted.

### 2.3. In-situ Raman spectroscopy

For the collection of *in-situ* Raman spectra of the sample in different environmental conditions, the Horiba-Jobin Yvon LabRam HR instrument was utilized. The details of the instrument is described elsewhere. [12] In the current investigation, approximately 25–30 mg of the sample (in powder form) was loaded in the sample cup of the Linkam CCR 1000 environmental cell with a quartz window and O-ring seal. For all spectra collection, the 532 nm laser was utilized.

At first, the sample was dehydrated at 400  $^{\circ}\text{C}$  under flowing 10 %  $O_2/$  Ar ( $\sim\!30$  cc/min) for 1 h. Subsequently, a dehydrated spectrum was collected at 400  $^{\circ}\text{C}$ . The sample was then heated to 900  $^{\circ}\text{C}$  (at 10  $^{\circ}\text{C}/$  min), followed by another spectrum collection. Then the gas environment was switched to the OCM conditions (CH<sub>4</sub>:O<sub>2</sub>:N<sub>2</sub> 3.3:1:4, total flow  $\sim\!65$  cc/min). After treatment of the sample at 900  $^{\circ}\text{C}$  for 2 h, in the OCM gas mixture, another spectrum was collected. The sample was cooled down in the same OCM gas flow to enhance the spectral resolution and avoid thermal broadening, and two more spectra were collected at 400  $^{\circ}\text{C}$  and 120  $^{\circ}\text{C}$ .

### 2.4. H<sub>2</sub>-TPR

The  $H_2$ -TPR experiments were conducted in a Micromeritics® AutoChem II instrument equipped with a TCD detector. For each experiment, about 100 mg of the catalyst sample was used. For  $H_2$ -TPR of freshly calcined catalysts, the catalyst samples were first dehydrated in 10 %  $O_2$ /Ar ( $\sim$ 30 cc/min) at 400 °C for 1 h, then cooled down to 100 °C, followed by flushing with pure Ar ( $\sim$ 30 cc/min) for 30 mins. To conduct  $H_2$ -TPR on the OCM reaction mixture treated catalyst, the sample was first dehydrated at 400 °C under flowing 10 %  $O_2$ /Ar ( $\sim$ 30 cc/min) for 1 h, followed by heating to 900 °C. At 900 °C, the gas environment was switched to  $CH_4 + O_2 + N_2$  (3.3:1:4, total flow  $\sim$ 65 cc/min), and the sample was conditioned for 2 h. Subsequently, the sample was cooled down to 100 °C, followed by flushing with Ar ( $\sim$ 30 cc/min) for 30 mins. After the pre-treatment steps, the  $H_2$ -TPR experiments were then performed by ramping the temperature of the catalyst bed in 10 %  $H_2$ /Ar (30 cc/min) at a rate of 10 °C/min from 100° to 1000 °C.

For the cyclic H<sub>2</sub>-TPR experiment, the reduced samples were reoxidized *in-situ* at 900 °C, in the flow of OCM gas mixture (CH<sub>4</sub> +O<sub>2</sub> +N<sub>2</sub> 3.3:1:4, total flow  $\sim$ 65 cc/min) for 2 h. Subsequently, the sample was cooled down to 100 °C, followed by flushing with Ar ( $\sim$ 30 cc/min) for 30 mins. Finally, the H<sub>2</sub>-TPR experiment was performed on the reoxidized catalysts as described above.

The number of lattice O-atoms removed for each TPR experiment was calculated by finding the area under the respective TPR profiles and calibrating against the reduction profile of known amounts of CuO standard [36] (see Fig. S2 and associated details).

### 2.5. TAP experiments

The transient kinetic experiments were conducted in a TAP 3 instrument, Mithra Technologies. Three different types of TAP pump-probe experiments were conducted in this study. For these experiments, 50 %  $O_2/He$ , 50 %  $^{13}\text{CH}_4/\text{Ar}$ , 50 %  $C_2H_6/\text{Ar}$  and 50 %  $C_2H_4/\text{Ar}$  gases were utilized. The details of the reaction gas mixture procurement and blending procedures are described elsewhere. [15].

Approximately 25 mg of the catalyst sample was loaded into a quartz

micro-reactor (I.D. 4 mm, Length 38 mm) between inert quartz particles of size 250–300  $\mu m$ . Next, the catalyst bed was evacuated to  $\sim 4 \times 10^{-6}$ Pa, followed by heating to 800 °C (10 °C/min), with continuous pulsing of O2/He and held at 800 °C for 30 mins. After pretreatment of the catalyst samples, pump-probe experiments were conducted according to the details below. In each case, the pump-probe spacing between the O<sub>2</sub>/ He and  $^{13}$ CH<sub>4</sub>/Ar (or C<sub>2</sub>H<sub>6</sub>/Ar or C<sub>2</sub>H<sub>4</sub>/Ar) gas was maintained at 2 s. This ensures complete removal of gas-phase O<sub>2</sub> before the introduction of reactant gas into the catalyst bed. Thus, the products obtained in these experiments are not influenced by any gas phase oxygen pulse associated with the pump pulse. The detection of different gases was conducted using a mass-spectrometer (SRS RGA 200), situated at the exit of the micro-reactor. Also, in each case, calibration gas mixtures were utilized to determine the mass fragmentation pattern of each reactant and product gas for deconvolution of the overlapping masses. All pumpprobe experiments were conducted outside the Knudsen diffusion regime. For each experiment, data were presented by taking average of 15-25 pulse responses. The product yields of different catalysts were normalized by the respective BET surface area for fair comparison.

### • O<sub>2</sub>-<sup>13</sup>CH<sub>4</sub> pump-probe experiments

 $^{13}$ CH<sub>4</sub> isotope gas was utilized to better distinguish CO and C<sub>2</sub> products. For these experiments, the O<sub>2</sub>/He and  $^{13}$ CH<sub>4</sub>/Ar pulse sizes were approximately maintained  $\sim$  (2.15  $\pm$  0.05) x  $10^{-8}$  moles/pulse and (8.75  $\pm$  0.05) x  $10^{-8}$  moles/pulse, respectively. For species identification, m/z of 40 (Ar); 17 ( $^{13}$ CH<sub>4</sub>); 29 ( $^{13}$ CO); 30 ( $^{13}$ C<sub>2</sub>H<sub>6</sub>); 32 (O<sub>2</sub>) and 45 ( $^{13}$ CO<sub>2</sub>) were utilized.

### • O<sub>2</sub>-C<sub>2</sub>H<sub>6</sub> and O<sub>2</sub>-C<sub>2</sub>H<sub>4</sub> pump-probe experiments

For  $O_2$ - $C_2H_6$  pump-probe experiments,  $O_2$ /He and  $C_2H_6$ /Ar pulse sizes were approximately maintained  $\sim (3.25\pm0.05)$  x  $10^{-9}$  moles/pulse and  $(3.25\pm0.05)$  x  $10^{-8}$  moles/pulse, respectively, and m/z values of 40 (Ar); 26 ( $C_2H_4$ ); 28 (CO); 30 ( $C_2H_6$ ); 32 ( $O_2$ ) and 44 ( $CO_2$ ) were utilized for species identification. For the  $O_2$ - $C_2H_4$  pump-probe experiment,  $O_2$ /He and  $^{13}$ CH<sub>4</sub>/Ar pulse sizes were approximately maintained  $\sim (4.2\pm0.1)$  x  $10^{-9}$  moles/pulse and  $(4.1\pm0.1)$  x  $10^{-8}$  moles/pulse, respectively and m/z values of 40 (Ar); 26 ( $C_2H_4$ ); 28 (CO); 32 ( $O_2$ ) and 44 ( $CO_2$ ) were utilized for species identification.

### 2.6. Steady state experiments

Steady-state OCM reaction studies were conducted in a tubular fixed-bed quartz reactor (I.D. 6 mm and half-length 180 mm). A quartz frit was located at the middle of the tube. For each experiment, approximately 100 mg of catalyst sample was loaded onto the quartz frit. Then the remaining empty space inside the tube was filled with quartz beads (500–700  $\mu m$ ) to minimize the contribution from gas-phase reactions. The loaded tube was then placed in a programmable electric furnace. The temperature of the catalyst bed was monitored by a thermocouple (secured inside a quartz thermowell) placed directly above the catalyst bed.

Prior to any reaction, the catalyst sample was first heated to the desired reaction temperature (750, 775 or 800 °C) at a rate of 10 °C/ min, under a flowing  $O_2$  ( $\sim$  10 cc/min) and  $N_2$  ( $\sim$  40 cc/min) gas mixture and held at the reaction temperature for  $\sim$  30 min. Then the reactant gas mixture,  $CH_4$ ,  $O_2$ , diluted in  $N_2$ , was introduced (at different ratios and space velocities) into the reactor. The reaction was maintained at each condition for  $\sim$  3 h to ensure that steady-state conditions were achieved. The water vapor produced during the reaction was removed by cooling the exit gas mixture in a condenser at 0 °C. Gases were analyzed using online gas chromatography (GC System 2010, Shimadzu Technology), equipped with a flame ionization detector (GC-FID) and two thermal conductivity detectors (GC-TCD1 and GC-TCD2). The GC-TCD1 detector was equipped with Carboxen® 1010 PLOT

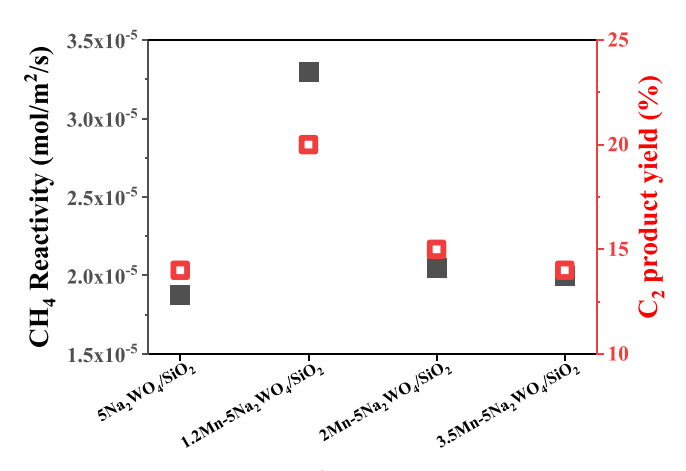


Fig. 1. The  $CH_4$  reactivity (mol/m<sup>2</sup> cat/s) obtained from steady-state OCM experiments over supported Mn-Na<sub>2</sub>WO<sub>4</sub>/SiO<sub>2</sub> catalysts. Reaction temperature 800 °C, gas space velocity 48 L/g cat/h and  $CH_4:O_2:N_2$  50:15:35. The corresponding  $CH_4$  conversion and product selectivity values are shown in Table S2.

(SUPLECO Analytical, Catalogue number 25467) fused silica capillary column to separate CO<sub>2</sub>,  $C_2H_2$ ,  $C_2H_4$  and  $C_2H_6$ . The GC-TCD2 detector is equipped with HP-PLOT Molesieve column (Agilent J&W GC Columns, Part number 19095 P-MSO) to separate O<sub>2</sub>, N<sub>2</sub>, CH<sub>4</sub> and CO. Both GC-TCD1 and GC-TCD2 detectors use He as carrier gas. The GC calibration was done using calibration gas mixtures in a 5-point calibration method. For data analysis, an average of 5–6 data points were utilized in each case.

 $CH_4$ ,  $O_2$  conversion and CO,  $CO_2$ ,  $C_2H_6$  and  $C_2H_4$  selectivity and yield values were obtained by the following formulae (Eqs. 1–3):

% Conversion = 
$$\frac{(F_i - F_o)}{F_i} \times 100$$
 (1)

where,  $F_i$  and  $F_o$  are the inlet and outlet molar flow rates (mol/s), respectively, of CH<sub>4</sub> or O<sub>2</sub>.

% Selectivity<sub>j</sub> = 
$$\frac{n_{C_j}}{\sum n_{C_i}} \times 100$$
 (2)

where,  $n_{C_i}$  is the number of moles of carbon atoms in product j.

% 
$$Yield_j = \frac{\% CH_4 Conversion \times \% Selectivity_j}{100}$$
 (3)

### 3. Results

### 3.1. Mn loading for optimum OCM catalytic performance

The general consensus in the OCM literature is that 2 wt % Mn loading is optimum for giving the highest catalytic OCM performance of supported Mn-5Na<sub>2</sub>WO<sub>4</sub>/SiO<sub>2</sub> catalysts, although the Mn loading between 0.5 and 3 wt % (on metal basis) can be considered the best. [5] The very first publication that systematically studied the effect of active metal oxide phases found 1 wt % Mn loading gave the best OCM performance. [26] Subsequently, another study reported the 2 wt % Mn loading to have the highest OCM activity. [37] The large variation in the optimum Mn loading can be attributed to the catalyst synthesis approach and/or parameters utilized for conducting the reaction studies. This observation compelled us to explore different Mn loadings for our supported Mn-5Na<sub>2</sub>WO<sub>4</sub>/SiO<sub>2</sub> catalysts.

Supported Mn-5Na<sub>2</sub>WO<sub>4</sub>/SiO<sub>2</sub> catalysts with three different Mn loadings (1.2, 2 and 3.5 wt %) were prepared. The corresponding BET surface area and catalytic performance are presented in Table S1, Table S2 and Fig. 1. All catalysts possess similar surface areas ( $\sim$ 3–4 m<sup>2</sup>/g). The addition of a small amount of Mn (1.2 wt %) increases the CH<sub>4</sub> activity and C<sub>2</sub> product selectivity of supported 5Na<sub>2</sub>WO<sub>4</sub>/SiO<sub>2</sub> catalyst

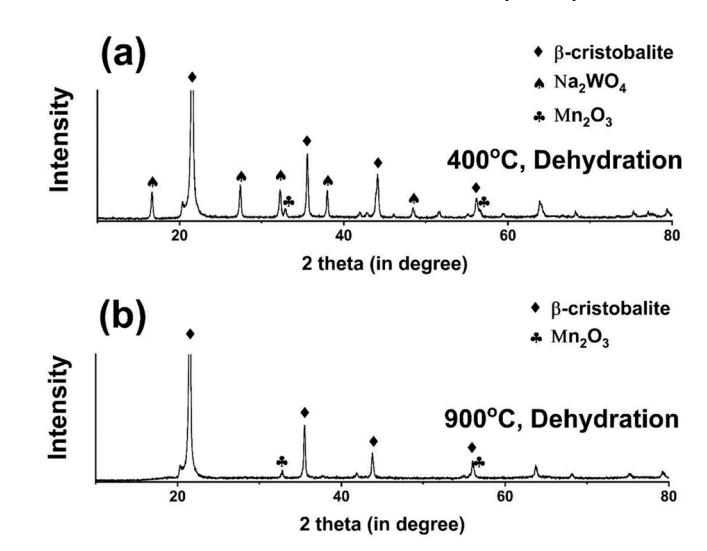


Fig. 2. In-situ XRD spectra of  $1.2Mn-5Na_2WO_4/SiO_2$  catalyst under dehydrated conditions at (a) 400 °C and (b) 900 °C.

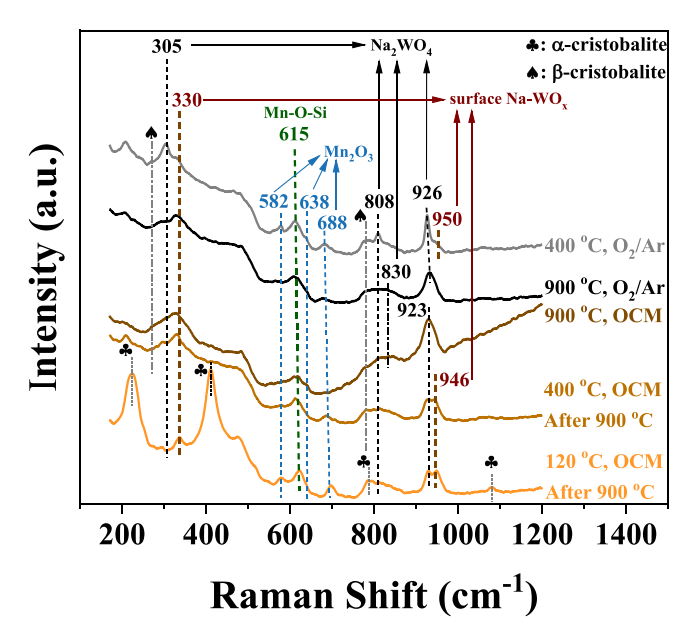


Fig. 3. In-situ Raman spectra of supported  $1.2 Mn-5 Na_2 WO_4/SiO_2$  catalyst in different environmental conditions.

by 35–40 %. The addition of higher amounts of Mn (2 and 3.5 wt %), however, does not significantly improve the catalytic OCM performance. Thus, for the current investigation the  $1.2 \text{Mn-}5 \text{Na}_2 \text{WO}_4/\text{SiO}_2$  catalyst was chosen as the representative catalyst to study the role and promotional effect of Mn. The performance of  $5 \text{Na}_2 \text{WO}_4/\text{SiO}_2$  and  $1.2 \text{Mn/}\text{SiO}_2$  catalysts will be discussed as needed for better understanding of the Mn promotional effect.

### 3.2. In-situ XRD

The *in-situ* XRD spectra of the supported 1.2Mn-5Na<sub>2</sub>WO<sub>4</sub>/SiO<sub>2</sub> catalyst are presented in Fig. 2. The spectrum of the dehydrated catalyst at 400 °C shows the presence of the crystalline Na<sub>2</sub>WO<sub>4</sub>, Mn<sub>2</sub>O<sub>3</sub> and  $\beta$ -cristobalite (SiO<sub>2</sub>) phases. Upon increasing the temperature to 900 °C, only the crystalline Mn<sub>2</sub>O<sub>3</sub> and the  $\beta$ -cristobalite (SiO<sub>2</sub>) phases are observed, and the Na<sub>2</sub>WO<sub>4</sub> crystalline phase is no longer detected.

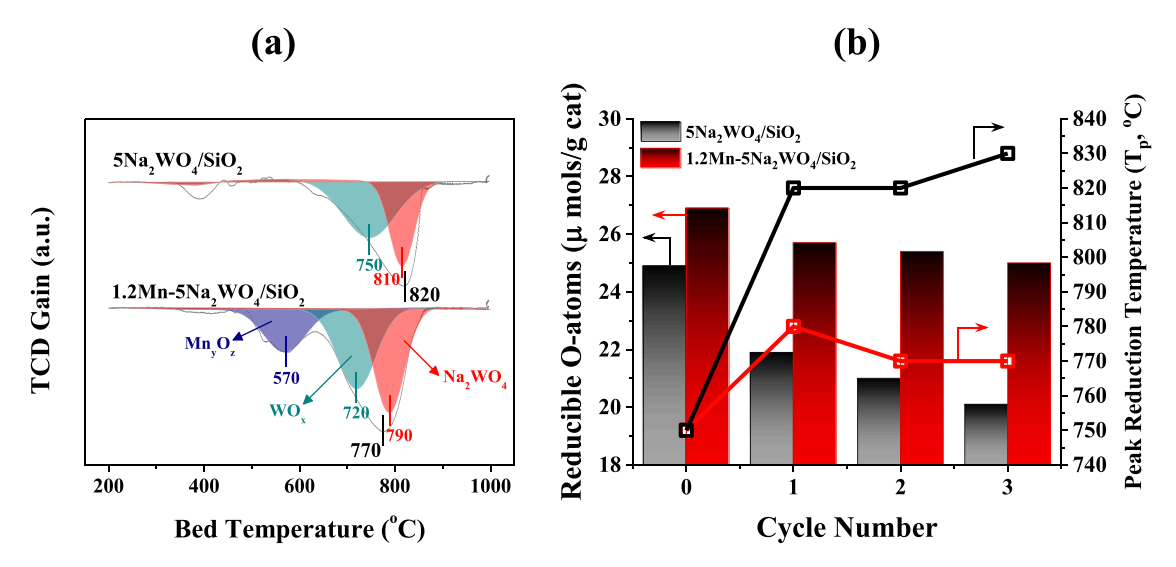


Fig. 4. (a)  $H_2$ -TPR profiles of supported  $5Na_2WO_4/SiO_2$  and the  $1.2Mn-5Na_2WO_4/SiO_2$  catalysts after treatment in OCM reaction conditions. (b) Quantified lattice O-atoms removed and peak reduction temperatures (associated with only the reduction of W-oxide phases: surface  $Na-WO_x$  and  $Na_2WO_4$ ) for freshly calcined (Cycle Number 0), OCM reaction mixture treated (Cycle Number 1) and reoxidized (Cycle Number 2 and 3) supported  $5Na_2WO_4/SiO_2$  and the supported  $1.2Mn-5Na_2WO_4/SiO_2$  catalysts.

#### 3.3. In-situ Raman spectroscopy

<code>In-situ</code> Raman experiments were conducted to complement the <code>in-situ</code> XRD findings (i.e., to identify oxide phases lacking long range order and small NPs (<3 nm in size)) to fully understand the structural dynamics of the supported 1.2Mn-5Na $_2$ WO $_4$ /SiO $_2$  catalyst in oxidizing and OCM reaction environments (see Fig. 3).

### 3.3.1. In-situ Raman spectra in oxidizing environments

The Raman spectrum of the dehydrated 1.2Mn-5Na<sub>2</sub>WO<sub>4</sub>/SiO<sub>2</sub> catalyst at 400  $^{\circ}$ C (in O<sub>2</sub>/Ar environment) exhibits three bands at 926, 808 and  $305\,\mathrm{cm}^{-1}$  associated with the vibrations of the crystalline Na<sub>2</sub>WO<sub>4</sub> phase. [13,15,16,38] The Raman bands at 582, 638 and 688 cm<sup>-1</sup> arise from the vibrations of the Mn<sub>2</sub>O<sub>3</sub> crystalline phase. [39, 40] Apart from the crystalline phases, two more Raman vibrations at 950 and 330 cm $^{-1}$  are present from surface Na-WO<sub>x</sub> sites. [12,14,15,41] Another strong band is observed ~615 cm<sup>-1</sup> that is absent for the Mn-free supported 5Na<sub>2</sub>WO<sub>4</sub>/SiO<sub>2</sub> catalyst, [12,15] which indicates it originates from the presence of Mn-oxide. This vibration does not match with any of the crystalline Mn-oxide phases or the crystalline MnWO<sub>4</sub> phase. [39,42] The band at  $\sim$ 615 cm<sup>-1</sup> is also quite different and far more intense than the vibration from the SiO<sub>2</sub> defect mode. [43] Based on these comparisons, the Raman band at  $\sim$ 615 cm<sup>-1</sup> is assigned to the vibration of the Mn-O-Si bond from surface MnO<sub>x</sub> species on the SiO<sub>2</sub> support. A similar vibrational band has been observed from Raman spectroscopy of supported MnO<sub>x</sub>/SiO<sub>2</sub> catalysts. [14,44].

Further heating the catalyst to 900 °C in an  $O_2/Ar$  environment results in disappearance of the 808 and 305 cm<sup>-1</sup> bands of crystalline  $Na_2WO_4$ , whereas the intensity of the 926 cm<sup>-1</sup> band from crystalline  $Na_2WO_4$  is observed to decrease with noticeable broadening. A new band at ~830 cm<sup>-1</sup> also appears, which is from asymmetric W=O vibration of the molten  $Na_2WO_4$  phase. [45] In contrast, Raman vibrations from the surface  $Na_2WO_4$  phase. [45] In contrast, Raman vibrations from the surface  $Na_2WO_4$  sites (330 cm<sup>-1</sup> and ~946 cm<sup>-1</sup>, shoulder of 926 cm<sup>-1</sup> band), crystalline  $Mn_2O_3$  (582, 638 and 688 cm<sup>-1</sup>), and  $Mn_2O_3$  (615 cm<sup>-1</sup>) are present at 900 °C in the oxidizing environment, although with noticeable thermal broadening.

### 3.3.2. In-situ Raman spectra in an OCM environment

Switching the gas flow to an OCM reaction mixture at 900  $^{\circ}$ C results in complete disappearance of the Raman vibrations from the crystalline  $Mn_2O_3$  phase (582, 638 and 688 cm $^{-1}$ ), but the Raman vibrations from

the surface Na-WO<sub>x</sub> sites (330 cm $^{-1}$  and  $\sim$ 946 cm $^{-1}$ ) and surface Mn-O-Si sites (615 cm $^{-1}$ ) remain at 900 °C under the OCM environment.

Upon cooling to lower temperatures (400 °C and then to 120 °C in the OCM gas mixture), the Raman bands from the crystalline Na<sub>2</sub>WO<sub>4</sub> and Mn<sub>2</sub>O<sub>3</sub> phases reappear with the Raman bands shifting from 926 to 923 cm $^{-1}$  and 950–946 cm $^{-1}$ . Additionally, the relative intensity of Raman bands from the crystalline Na<sub>2</sub>WO<sub>4</sub> phase (923 and 305 cm $^{-1}$ ) significantly decreases in comparison to the Raman vibrations from the surface Na-WO<sub>x</sub> sites (946 and 330 cm $^{-1}$ , respectively) after treatment under the OCM reaction conditions. No change in the Mn-O-Si vibration at 615 cm $^{-1}$  is noticed. The crystalline  $\beta$ - to  $\alpha$ -cristobalite phase transformation of the SiO<sub>2</sub> support is also observed for the 400 and 120 °C spectra, respectively.

### 3.4. H<sub>2</sub>-TPR

The  $\rm H_2$ -TPR spectra of freshly dehydrated and OCM reaction treated supported 1.2Mn-5Na<sub>2</sub>WO<sub>4</sub>/SiO<sub>2</sub> catalysts are shown in Fig. S3 and Fig. 4. To understand the effect of MnO<sub>x</sub> promotion, the corresponding H<sub>2</sub>-TPR data obtained for the 5Na<sub>2</sub>WO<sub>4</sub>/SiO<sub>2</sub> catalysts are also included for comparison.

Supported 5Na<sub>2</sub>WO<sub>4</sub>/SiO<sub>2</sub> catalyst: The H<sub>2</sub>-TPR of the freshly calcined supported 5Na<sub>2</sub>WO<sub>4</sub>/SiO<sub>2</sub> catalyst exhibits a peak ~750 °C (see Fig. S3). After treatment in OCM reaction conditions, the reduction peak shifts to a higher temperature ( $\sim 820$  °C). A better analysis of reduction from different oxide phases is presented in Fig. 4(a). Two distinct reduction regimes can be observed for the supported 5Na<sub>2</sub>WO<sub>4</sub>/SiO<sub>2</sub> catalyst. The surface Na-WOx sites (green highlighted area) reduce at a lower temperature than the corresponding Na<sub>2</sub>WO<sub>4</sub> NPs (red highlighted area). [12,15] The lattice O-atoms removed, along with the corresponding reduction peak temperatures for freshly calcined, OCM reaction mixture treated and in-situ reoxidized supported 5Na<sub>2</sub>WO<sub>4</sub>/-SiO<sub>2</sub> catalysts are shown in Fig. 4(b). The peak reduction temperature increases and the amount of lattice O-atoms modestly decreases: freshly calcined (750  $^{\circ}\text{C},\,\sim\,25\,\mu\text{mol/g}$  cat)  $\rightarrow\,$  OCM reaction mixture treated (820 °C, < 22  $\mu$ mol/g cat)  $\rightarrow$  in-situ reoxidized (830 °C, < 20  $\mu$ mol/g cat) 5Na<sub>2</sub>WO<sub>4</sub>/SiO<sub>2</sub> catalysts.

**Supported 1.2Mn-5Na<sub>2</sub>WO<sub>4</sub>/SiO<sub>2</sub> catalyst:** The reduction peak for the freshly calcined 1.2Mn-5Na<sub>2</sub>WO<sub>4</sub>/SiO<sub>2</sub> catalyst is  $\sim$ 750 °C, which demonstrated a minor increase towards higher temperature ( $\sim$ 770 °C) after treatment in the OCM reaction mixture (see Fig. S3). Similar to the

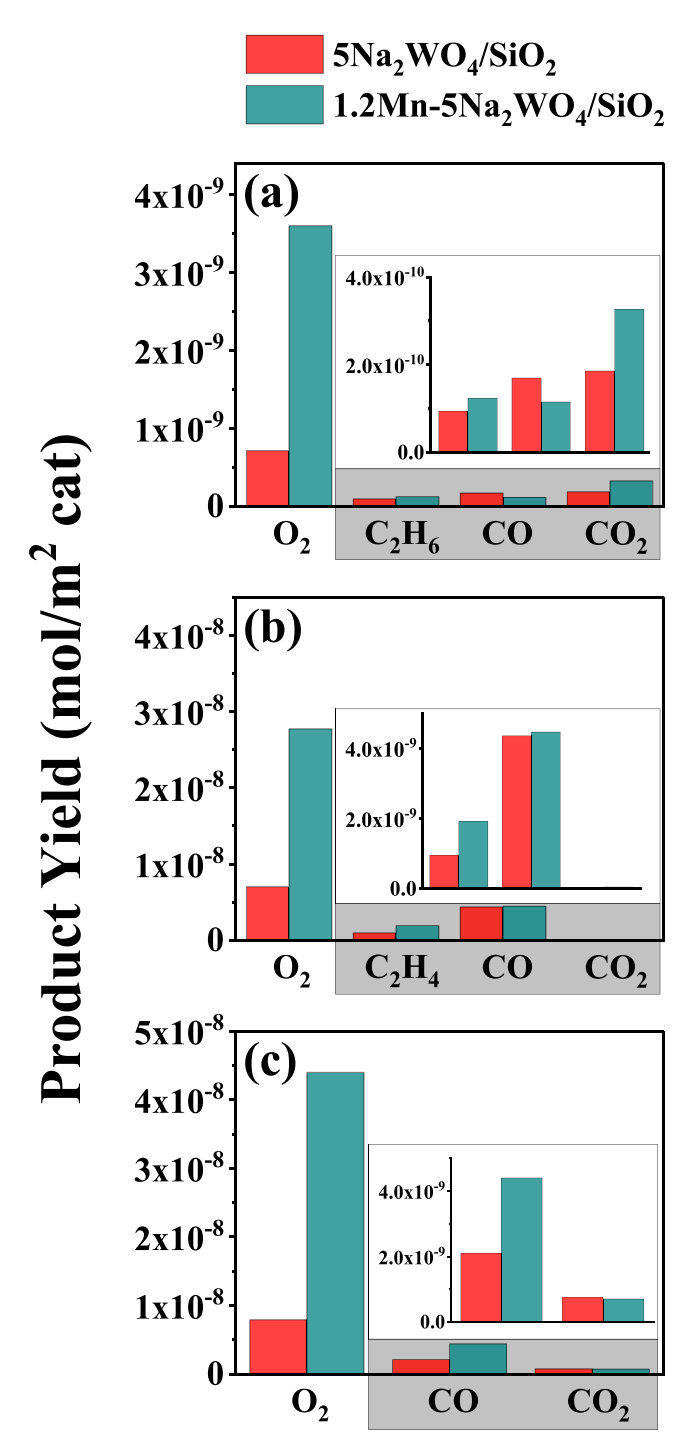


**Fig. 5.** Product formation associated with the secondary (probe) pulse of TAP. a)  $O_2$ - $^{13}$ CH<sub>4</sub>, b)  $O_2$ - $O_2$ -

supported  $5Na_2WO_4/SiO_2$  catalyst, two separate reduction regimes, from surface Na- $WO_x$  sites and  $Na_2WO_4$  NPs, are present for the supported 1.2Mn- $5Na_2WO_4/SiO_2$  catalysts at higher temperatures (see Fig. 4(a)). An additional reduction peak is present at  $\sim 570$  °C that is assigned to the reduction of surface  $MnO_x$  species. [46,47] The peak reduction temperature (from  $750^\circ$  to 770 °C) and removable lattice O-atoms (from 27 to 25  $\mu$ mol/g cat,  $\sim 7$  % change) change (slightly

Table 1 Steady state OCM performance of multiple supported catalysts and quartz bed at  $800\,^{\circ}\text{C}$ ,  $\text{CH}_4\text{:}O_2\text{:}N_2$  50:15:35. The gas-space velocities are mentioned in the table

Gas-space Velocity (L/g cat/h)	CH <sub>4</sub> conversion (%)	C <sub>2</sub> selectivity (%)	C <sub>2</sub> H <sub>4</sub> /C <sub>2</sub> H <sub>6</sub> yield ratio
1.2 Mn/SiO <sub>2</sub>			
120	12.1	50	0.7
72	14.1	48	1
48	16.2	45	1.4
5Na <sub>2</sub> WO <sub>4</sub> /SiO <sub>2</sub>			
120	14.6	69	0.85
72	21.6	59	1.5
48	24.8	57	2.4
$1.2Mn\text{-}5Na_2WO_4/SiO_2$			
120	14.8	72	1
72	28.5	61	3.1
48	34.9	58	5.4
Quartz bed			
120	2.6	78	0.28
72	3.3	71	0.48
48	6.8	62	1.1

increase and decrease, respectively) in going from freshly calcined  $\rightarrow$  OCM reaction mixture treated  $\rightarrow$  *in-situ* reoxidized supported 1.2Mn-5Na<sub>2</sub>WO<sub>4</sub>/SiO<sub>2</sub> catalysts (see Fig. 4(b)).

### 3.5. TAP studies

TAP pump-probe experiments were conducted over the  $5\mathrm{Na}_2\mathrm{WO}_4/\mathrm{SiO}_2$  and  $1.2\mathrm{Mn}\text{-}5\mathrm{Na}_2\mathrm{WO}_4/\mathrm{SiO}_2$  catalysts to understand the promotional effect of  $\mathrm{MnO}_x$  on the OCM surface reaction network. It has been previously shown that the molten  $\mathrm{Na}_2\mathrm{WO}_4$  phase in  $\mathrm{Na}_2\mathrm{WO}_4/\mathrm{SiO}_2$  catalyst possesses dissolved molecular oxygen species at OCM relevant temperature which desorbs with the introduction of a secondary probe pulse. [15,35] Furthermore, the amount of molecular dioxygen released from the  $\mathrm{Na}_2\mathrm{WO}_4/\mathrm{SiO}_2$  catalyst increases in the presence of  $\mathrm{MnO}_x$  species. [35] In agreement with this finding, a higher amount of dioxygen release, during the probe pulse, was found for the supported  $1.2\mathrm{Mn}\text{-}5\mathrm{Na}_2\mathrm{WO}_4/\mathrm{SiO}_2$  catalyst for all pump-probe experiments (see Fig. 5).

For the  $O_2$ - $^{13}$ CH<sub>4</sub> pump-probe experiment, the addition of MnO<sub>x</sub> only results in a slight change in formation of  $C_2$ H<sub>6</sub> (slightly increased) and CO (slightly decreased). In contrast, a significant increase (~40 %) in the yield of CO<sub>2</sub> is noticed after MnO<sub>x</sub> addition (see Fig. 5(a)). For the  $O_2$ - $C_2$ H<sub>6</sub> pump-probe experiment, MnO<sub>x</sub> addition does not change the yield of CO and CO<sub>2</sub>. In contrast, the  $C_2$ H<sub>4</sub> yield almost doubles due to MnO<sub>x</sub> promotion. Finally, for  $O_2$ - $C_2$ H<sub>4</sub> pump-probe experiment, MnO<sub>x</sub> addition increases the CO formation and does not affect the CO<sub>2</sub> yield.

### 3.6. Steady state reaction studies

Steady state OCM reaction studies were carried out to complement the transient TAP experimental findings in order to gain additional insights into the role and promotion of  $MnO_x$  species for the OCM reaction. (see Table 1, Fig. 6 and Fig. 7).

The supported 1.2MnO<sub>x</sub>/SiO<sub>2</sub> catalyst is active for the OCM reaction, but yields low C<sub>2</sub> selectivity (Table 1). The supported  $5\text{Na}_2\text{WO}_4/\text{SiO}_2$  catalyst exhibits higher activity and C<sub>2</sub> product selectivity than the supported 1.2Mn/SiO<sub>2</sub> catalyst, especially for low gas-space velocities. The addition of Mn to the supported  $5\text{Na}_2\text{WO}_4/\text{SiO}_2$  catalyst (1.2Mn- $5\text{Na}_2\text{WO}_4/\text{SiO}_2$  catalyst) significantly improves the CH<sub>4</sub> activity without compromising the C<sub>2</sub> selectivity and also increases the ratio of C<sub>2</sub>H<sub>4</sub>/C<sub>2</sub>H<sub>6</sub> (1.2Mn/SiO<sub>2</sub> <  $5\text{Na}_2\text{WO}_4/\text{SiO}_2$  <  $1.2\text{Mn}_5\text{Na}_2\text{WO}_4/\text{SiO}_2$ ).

The effect of  $MnO_x$  on the supported  $5Na_2WO_4/SiO_2$  catalyst for CH<sub>4</sub> activity and product selectivity is a strong function of the reaction conditions (see Table 1). Steady state OCM reactions over the supported  $5Na_2WO_4/SiO_2$  and  $1.2Mn-5Na_2WO_4/SiO_2$  catalysts were conducted

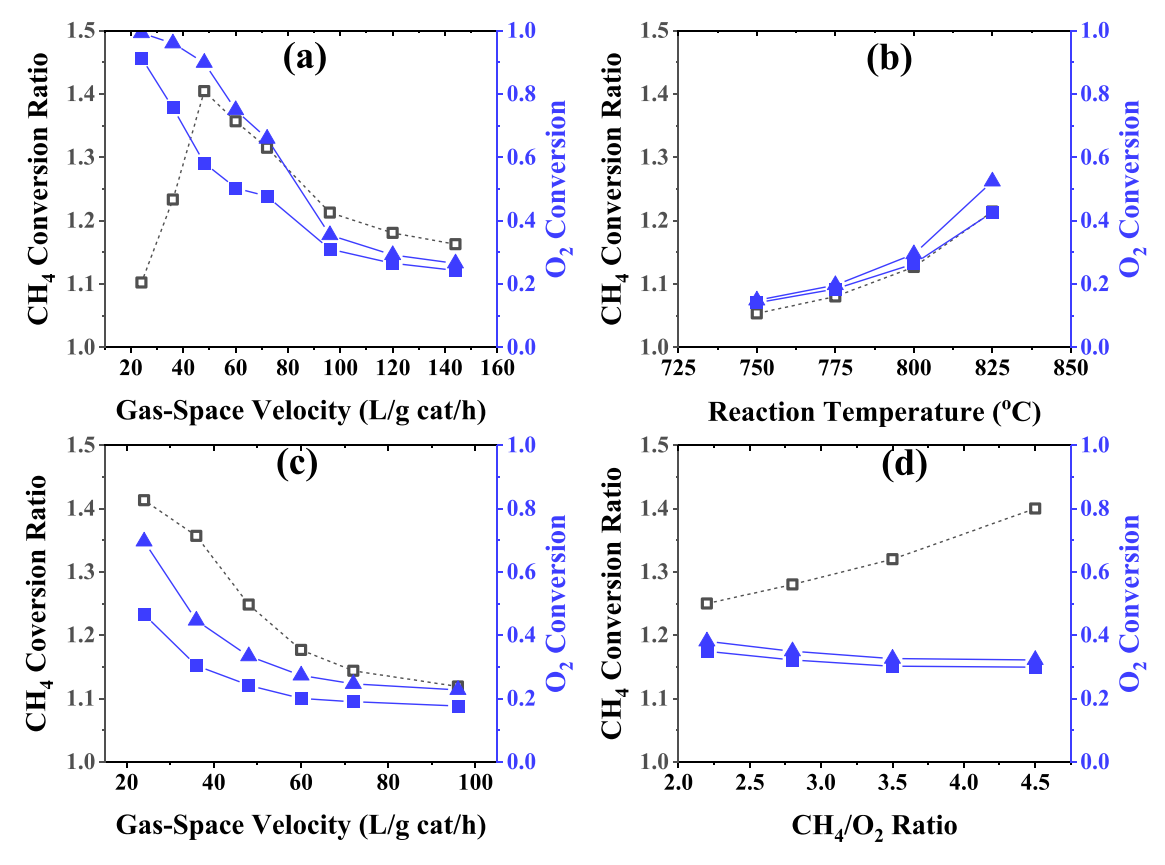


Fig. 6. The CH<sub>4</sub> Conversion Ratio of  $1.2Mn-5NaWO_4/SiO_2$  to  $5NaWO_4/SiO_2$  catalyst (empty black square) is shown for different reaction conditions, (a) 800 °C, varying gas-space velocity,  $CH_4:O_2:N_2$  50:15:35, (b) varying reaction temperature at a fixed gas-space velocity of 72 L/g cat/h,  $CH_4:O_2:N_2$  50:15:35, (c) 750 °C, varying gas-space velocity,  $CH_4:O_2:N_2$  50:15:35, and (d) 800 °C, gas-space velocity 60 L/g cat/h, varying  $CH_4/O_2$  ratio at a fixed  $CH_4$  partial pressure of 0.3. The corresponding  $O_2$  Conversion for  $1.2Mn-5NaWO_4/SiO_2$  (solid blue triangle) and  $5NaWO_4/SiO_2$  (solid blue square) catalysts are also shown in the figure.

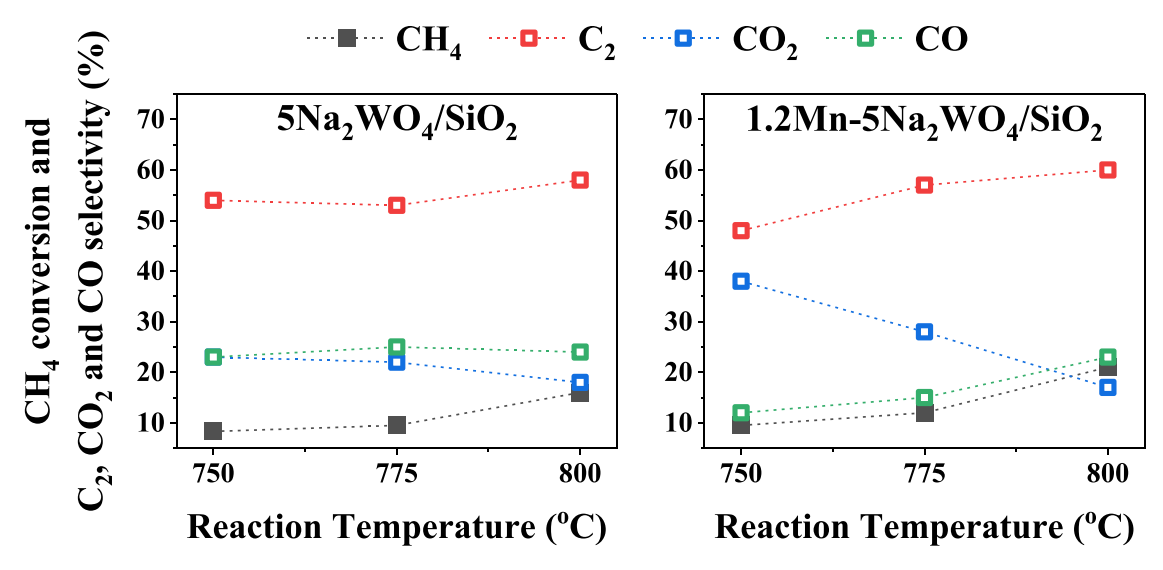


Fig. 7. The CH<sub>4</sub> conversion, and C<sub>2</sub>, CO<sub>2</sub> and CO selectivity of 5Na<sub>2</sub>WO<sub>4</sub>/SiO<sub>2</sub> and 1.2Mn-5Na<sub>2</sub>WO<sub>4</sub>/SiO<sub>2</sub> catalysts at varying reaction temperature at a fixed gasspace velocity of 72 L/g cat/h, CH<sub>4</sub>:O<sub>2</sub>:N<sub>2</sub> 50:15:35.

over a wide range of experimental conditions (gas-space velocity, temperature, and  $CH_4/O_2$  ratio) in order to gain deeper insight and the results are presented in Fig. 6. For better quantitative understanding, the effect of  $MnO_x$  is presented as the  $CH_4$  conversion ratio of the 1.2Mn- $5Na_2WO_4/SiO_2$  to  $5Na_2WO_4/SiO_2$  catalysts. The respective  $O_2$  conversion of these catalysts are also included in the Fig. 6.

Initially, the space velocity was varied at a fixed reaction

temperature (800  $^{\circ}$ C, see Fig. 6(a)). The effect of Mn becomes more pronounced (the CH<sub>4</sub> conversion ratio increases) up to a certain point and then decreases with decreasing space velocity. To understand this influence of Mn promotion behavior, the corresponding  $O_2$  conversion values were compared, and the observations can be summarized as follows:

- (i) At low  $O_2$  conversion values (high gas space velocities), sufficient gas-phase  $O_2$  is available for  $CH_4$  conversion and, consequently,  $MnO_x$  promotion does not significantly affect the  $CH_4$  conversion (conversion ratio is smaller).
- (ii) As the gas space velocity is progressively lowered, the conversion values of the reactants increase and the availability of gas phase  ${\rm O}_2$  diminishes. Under these conditions, the promotion by  ${\rm MnO}_x$  becomes more pronounced.
- (iii) As the gas space velocity is further lowered (the lowest two values in Fig. 6(a)), the CH $_4$  conversion ratio decreases because the  ${\rm O}_2$  conversion for the promoted supported 1.2Mn-5Na $_2$ WO $_4$ /SiO $_2$  catalyst approaches almost 100 %, and results in a lower CH $_4$  conversion and a lower CH $_4$  conversion ratio.

To further verify that the degree of  $MnO_x$  promotion is indeed dependent on the availability of the gas phase  $O_2$ , the same experiment was performed at a fixed space velocity and at varying temperatures (see Fig. 6(b)). As the gas-phase  $O_2$  conversion increases with temperature, the promotional effect of  $MnO_x$  also increases.

The effect of  $MnO_x$  promotion on  $CH_4$  activity was also investigated as a function of reaction temperature (see Fig. 6(a) and (c)). A simple comparison reveals that the effect of  $MnO_x$  promotion is even higher at a lower reaction temperature. For example, at similar  $O_2$  conversions (e.g., ~30 %) for the supported  $Na_2WO_4/SiO_2$  catalyst, the conversion ratio at 800 °C (~1.21) is lower than that at 750 °C (~1.36).

The effect of the  $CH_4/O_2$  ratio on  $MnO_x$  promotion was next examined (see Fig. 6(d)). The gas phase  $O_2$  conversion only slightly decreases for the range of  $CH_4/O_2$  ratios. The availability of gas phase oxygen, however, decreases significantly with increasing  $CH_4/O_2$  ratio due to the inherent nature of the experimental conditions imposed. Thus, the  $MnO_x$  promotion effect increases with increasing  $CH_4/O_2$  ratio.

The effect of  $MnO_x$  on OCM reaction product selectivity was also investigated as a function of reaction temperature and presented in Fig. 7. For the supported  $5Na_2WO_4/SiO_2$  catalyst, only small variations in the  $C_2$ ,  $CO_2$  and CO selectivity values were observed with changing reaction temperature while the  $CH_4$  conversions increased. For the supported  $1.2Mn-5Na_2WO_4/SiO_2$  catalyst, however, the  $C_2$  and CO selectivity values show a noticeable increase and  $CO_2$  selectivity drastically diminishes with increasing reaction temperature.

### 4. Discussion

### 4.1. Dynamics of supported Mn-Na<sub>2</sub>WO<sub>4</sub>/SiO<sub>2</sub> catalyst structure

Structure of supported Mn-Na<sub>2</sub>WO<sub>4</sub>/SiO<sub>2</sub> catalyst in oxidizing environments: The freshly calcined, dehydrated 1.2Mn-5Na<sub>2</sub>WO<sub>4</sub>/SiO<sub>2</sub> catalyst possesses crystalline Mn<sub>2</sub>O<sub>3</sub>, Na<sub>2</sub>WO<sub>4</sub> and  $\beta$ -cristobalite (SiO<sub>2</sub>) phases at 400 °C in an oxidizing environment (see Fig. 2 and Fig. 3). Surface Na-WO<sub>x</sub> and MnO<sub>x</sub> sites are also present on the SiO<sub>2</sub> support (see Fig. 3). The supported crystalline Na<sub>2</sub>WO<sub>4</sub> phase is not present at 900 °C (see Fig. 2 and Fig. 3) due to melting above 700 °C. [7–13,15–17] In contrast, the crystalline Mn<sub>2</sub>O<sub>3</sub> phase, and surface Na-WO<sub>x</sub> and MnO<sub>x</sub> sites are stable at 900 °C in an oxidizing environment.

Structure of supported Mn-Na<sub>2</sub>WO<sub>4</sub>/SiO<sub>2</sub> catalyst in OCM reaction environments: Under OCM reaction conditions (900 °C), only the molten Na<sub>2</sub>WO<sub>4</sub> phase and surface Na-WO<sub>x</sub> and MnO<sub>x</sub> sites are present on the  $\beta$ -cristobalite (SiO<sub>2</sub>) support (see Fig. 3). The crystalline Mn<sub>2</sub>O<sub>3</sub> phase, however, is absent under OCM (see Fig. 3). A previous *in-situ* Raman investigation on the bulk Mn<sub>2</sub>O<sub>3</sub> phase showed that at high temperature (> 500 °C) and under inert (only He flow) or reducing (CH<sub>4</sub>:O<sub>2</sub> 1:6) environment, the Mn<sub>2</sub>O<sub>3</sub> phase transforms to the Mn<sub>3</sub>O<sub>4</sub> phase upon reduction. [40] In the present study under OCM reaction at 900 °C, however, the Raman band for the crystalline Mn<sub>3</sub>O<sub>4</sub> phase (~650 cm<sup>-1</sup>) was not detected (see Fig. 3). [44] The absence of the crystalline Mn<sub>3</sub>O<sub>4</sub> phase could be due to thermal broadening at high OCM reaction temperature or simply because the crystalline Mn<sub>3</sub>O<sub>4</sub>

phase does not exist owing to a net reducing gas environment (CH<sub>4</sub>:O<sub>2</sub>:  $N_2$  3.3:1:4). The absence of crystalline Mn-oxide phase during OCM reaction is also in agreement with previous *in-situ* XRD studies. [11] (The NAP-XPS data (see Fig. S1) show that Mn is present as both Mn<sup>3+</sup> and Mn<sup>2+</sup> oxidation states in the OCM environment. However, the 600 °C temperature for the NAP-XPS measurement is below that required for the OCM reaction.) Upon cooling to lower temperatures (400 °C and 120 °C), the crystalline  $Mn_2O_3$  and  $Na_2WO_4$  phases reappear. The crystalline  $Mn_2O_3$  phase reappears because CH<sub>4</sub> is not able to reduce the  $Mn_2O_3$  phase at these lower temperatures, but  $Mn_3O_4$ , if present, can be oxidized by gas-phase molecular  $O_2$ . The crystalline  $Na_2WO_4$  phase reappears because these temperatures are below its melting point (~700 °C).

Differing conclusions can be found in the literature regarding the nature of manganese oxide phases in different gas environments and temperatures. In agreement with our findings, a few studies report the presence of the Mn<sub>2</sub>O<sub>3</sub> phase under oxidizing environments and OCM relevant temperatures. [7,16] In contrast, other studies observed the  $Mn_2O_3$  phase in oxidizing environments and only low temperatures. [9, 10] At high temperatures and oxidizing environments, the Mn<sub>2</sub>O<sub>3</sub> phase was seen to transform to the crystalline MnWO<sub>4</sub> phase during melting of Na<sub>2</sub>WO<sub>4</sub>. [9] Alternatively, the presence of large amounts of Mn<sub>2</sub>SiO<sub>12</sub> (with trace amount of MnWO<sub>4</sub>) is also reported to be present under oxidizing environments and OCM relevant temperature. [11,13] The current studies, however, did not detect the presence of crystalline Mn<sub>7</sub>SiO<sub>12</sub> or formation of the crystalline MnWO<sub>4</sub> phase in the oxidized supported 1.2Mn-5Na<sub>2</sub>WO<sub>4</sub>/SiO<sub>2</sub> catalyst (see Fig. 2 and Fig. 3). Under the OCM reaction environment, a few in-situ/operando XRD studies reported the disappearance of the crystalline Mn<sub>2</sub>O<sub>3</sub> phase, which is in agreement with the current findings (see Fig. 3). The formation of crystalline Mn<sub>2</sub>O<sub>3</sub> or Mn<sub>7</sub>SiO<sub>12</sub> phases were also detected during an inert or OCM reaction gas environment. [11,13] A possible reason for the formation of the crystalline Mn<sub>7</sub>SiO<sub>12</sub> phase may be related to the type of starting SiO<sub>2</sub> support used by different researchers. [48].

In summary, the current findings reveal that the oxide phases present for the supported  $1.2Mn-5Na_2WO_4/SiO_2$  catalyst under OCM reaction conditions are the molten  $Na_2WO_4$  phase and the surface  $Na-WO_x$  and  $MnO_x$  sites on the crystalline  $\beta$ -cristobalite (SiO<sub>2</sub>) support.

### 4.2. Formation of new surface Na-WO<sub>x</sub> sites on SiO<sub>2</sub> during OCM

Heating supported 1.2Mn-5Na<sub>2</sub>WO<sub>4</sub>/SiO<sub>2</sub> catalysts above the melting point of crystalline Na<sub>2</sub>WO<sub>4</sub> (~700 °C) also results in the formation of isolated surface Na-WO<sub>x</sub> sites (Raman bands at 950 and 330 cm<sup>-1</sup>, see Fig. 3). Consequently, both isolated surface Na-WO<sub>x</sub> sites and the molten Na<sub>2</sub>WO<sub>4</sub> phase (broad bands at 926, 808 and 305 cm<sup>-1</sup>) co-exist under OCM reaction conditions. Interestingly, the intensity of Raman vibrations from surface Na-WO<sub>x</sub> sites (946 and 330 cm<sup>-1</sup>) has increased considerably after treatment under OCM reaction conditions (see Fig. 3). Such relative increase in the intensity of surface Na-WO<sub>x</sub> species was also observed for the 5Na<sub>2</sub>WO<sub>4</sub>/SiO<sub>2</sub> catalyst. [15] Additionally, the O1s lines from the NAP-XPS experiments show that the relative intensity of the oxygen peak from active metal oxide phases considerably increases in comparison to the oxygen associated with the SiO<sub>2</sub> support (see Fig. S1 and associated discussion) after catalyst treatment under OCM reaction conditions. All the above observations and discussion suggest that new surface WO<sub>x</sub> sites are formed during OCM reaction.

### 4.3. Interaction between active metal oxide phases during OCM

Additional data processing was undertaken to examine the Raman shifts of the  $\rm Na_2WO_4$  phase (from 926 to 923 cm $^{-1}$ ) and surface  $\rm Na\text{-}WO_x$  sites (from 950 cm to 946 cm $^{-1}$ ) of the supported 1.2Mn-5Na<sub>2</sub>WO<sub>4</sub>/SiO<sub>2</sub> catalyst after exposure to the OCM reaction environment (see Fig. 3, Fig. S4 and associated discussion). The comparative analysis between

the supported 5Na<sub>2</sub>WO<sub>4</sub>/SiO<sub>2</sub> and 1.2Mn-5Na<sub>2</sub>WO<sub>4</sub>/SiO<sub>2</sub> catalysts suggest the interaction of Mn with both the molten Na<sub>2</sub>WO<sub>4</sub> phase and surface Na-WO<sub>x</sub> sites during OCM. The interaction of Mn with molten Na<sub>2</sub>WO<sub>4</sub> phase has previously been reported with in-situ Raman spectroscopy, in agreement with the current findings. [16] Furthermore, an in-situ Raman spectroscopic comparison of the supported 5WOx/SiO2 and 0.7Mn-3WO<sub>x</sub>/SiO<sub>2</sub> catalysts was undertaken to examine the possible interaction of MnO<sub>x</sub> with surface WO<sub>x</sub> sites (see Fig. S5 and associated discussion). The Raman spectra of the dehydrated catalysts showed the presence of surface Mn-WO<sub>x</sub> sites (~924 and 944 cm<sup>-1</sup>, perturbed from 984 and 1014 cm<sup>-1</sup> bands for the supported WO<sub>x</sub>/SiO<sub>2</sub> catalyst with additional presence of crystalline MnWO4 phase). This confirms that MnOx can interact with surface WOx sites on SiO2 and is reflected in perturbation of the W=O vibration of the surface WO<sub>4</sub> sites. To the best of our knowledge, the interaction between surface MnO<sub>x</sub> species and W-oxides (molten Na<sub>2</sub>WO<sub>4</sub> phase and surface Na-WO<sub>x</sub> sites) on SiO2 for supported Mn-Na2WO4/SiO2 catalysts during the OCM reaction has been shown, for the first time, via direct spectroscopic experiments.

The interaction of Mn with both the surface Na-WO $_{\rm X}$  sites and molten Na $_{\rm 2}$ WO $_{\rm 4}$  phase is also apparent from the H $_{\rm 2}$ -TPR experiments (see Fig. S3 and Fig. 4). The freshly calcined supported  $5{\rm Na}_{\rm 2}$ WO $_{\rm 4}$ /SiO $_{\rm 2}$  and 1.2Mn-5Na $_{\rm 2}$ WO $_{\rm 4}$ /SiO $_{\rm 2}$  catalysts exhibit similar TPR profiles. However, only the supported 1.2Mn-5Na $_{\rm 2}$ WO $_{\rm 4}$ /SiO $_{\rm 2}$  catalyst was able to maintain a constant peak reduction temperature and total number of reducible O-atoms after several cycles of oxidation reductions. Moreover, even for the fresh catalysts, the number of removable O-atoms (associated with both surface Na-WO $_{\rm X}$  species and Na $_{\rm 2}$ WO $_{\rm 4}$  phase) from 1.2Mn-5Na $_{\rm 2}$ WO $_{\rm 4}$ /SiO $_{\rm 2}$  catalyst is more than 10 % higher than the 5Na $_{\rm 2}$ WO $_{\rm 4}$ /SiO $_{\rm 2}$  catalyst. The above observations strongly support an interaction between Mn and W-oxide (surface Na-WO $_{\rm X}$  species as well as Na $_{\rm 2}$ WO $_{\rm 4}$  phase) and is consistent with previous literature findings [16,35].

# 4.4. Active site(s) in supported Mn-Na<sub>2</sub>WO<sub>4</sub>/SiO<sub>2</sub> catalyst for catalytic OCM reaction

Although the supported  $1.2 Mn/SiO_2$  catalyst is capable of activating  $CH_4$ , its  $C_2$  selectivity is significantly lower than that of the supported  $5Na_2WO_4/SiO_2$  catalysts (with or without Mn promotion). The addition of  $MnO_x$  to the supported  $5Na_2WO_4/SiO_2$  catalyst, however, significantly improves the  $CH_4$  reactivity without affecting the  $C_2$  selectivity (see Table 1). This suggests, in contrast to many proposals in the literature [7,24-28], that the Mn-oxide by itself cannot be the selective active center for the OCM reaction to form  $C_2$  product, but serves as a promoter for the supported  $5Na_2WO_4/SiO_2$  catalysts to improve catalytic OCM activity without compromising  $C_2$  selectivity. This observation also suggests that the W-oxide (surface  $Na-WO_x$  sites and molten  $Na_2WO_4$  phase) phases are the active sites for the catalytic OCM reaction [3,19-23,49].

### 4.5. Contribution of $MnO_x$ towards catalytic OCM reaction network

Deeper insights into the role of  $MnO_x$  in the catalytic OCM reaction network were gained from TAP experiments (see Fig. 5). The  $O_2$ - $^{13}CH_4$  pump-probe experiment revealed that the promotion with  $MnO_x$  significantly increases the total number of labile  $O_2$  released from the surface (associated with molten  $Na_2WO_4$  phase) from the  $5Na_2WO_4/SiO_2$  catalyst. [35] The production of  $C_2H_6$ , however, was minimally affected suggesting the surface  $Na_2WO_x$  sites are mostly responsible for the formation of the  $C_2H_6$  product. In contrast, the  $CO_2$  yield was significantly enhanced, relating its origin to the molten  $Na_2WO_4$  phase. The involvement of W-oxide phases towards  $CH_4$  activation in the OCM reaction is in agreement with many previous findings [3,16,19–23].

Further, the  $O_2$ - $C_2H_6$  pump-probe experiment showed significant improvement in  $C_2H_4$  production in the presence of Mn (and concomitant higher amount of released  $O_2$  from the molten  $Na_2WO_4$  phase),

suggesting that the molten  $Na_2WO_4$  phase is also responsible for oxidative dehydrogenation of  $C_2H_6$  to  $C_2H_4$ . [15] This result is also confirmed by the steady state OCM reaction studies (see Table 1). [15, 50] The reactivity data and product distribution suggest that (i) Mn-oxide is only modestly effective as a dehydrogenation center for  $C_2H_6$  to  $C_2H_4$  oxidative conversion since its dehydrogenation capability is even lower than the supported  $5Na_2WO_4/SiO_2$  catalyst, (ii) the addition of  $MnO_x$  to the supported  $5Na_2WO_4/SiO_2$  catalyst, however, improves the  $C_2H_4$  product selectivity that is related to a greater number of dioxygen species available from the molten  $Na_2WO_4$  phase.

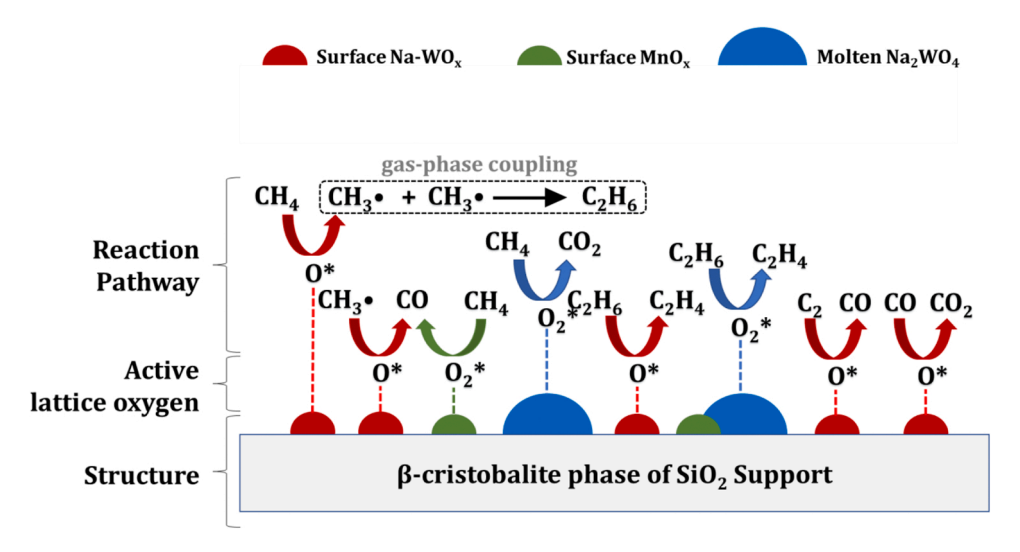
## 4.6. Influence of gas-phase molecular O<sub>2</sub> concentration on MnO<sub>x</sub> promotion

The catalytic OCM reaction over the supported 1.2Mn-5Na<sub>2</sub>WO<sub>4</sub>/  $SiO_2$  catalyst has been proposed to follow a hybrid Mars-van Krevelen redox type mechanism by many studies. [3,13,17,30-34,37] This suggests that the oxygen species from the active oxide phases becomes consumed in the oxidation reaction steps and then gets replenished by the gas phase oxygen. Thus, the OCM activity is expected to depend on both the gas phase O2 concentration and the exchange rate of oxygen between the gas phase and catalyst lattice. From catalytic OCM activity data in Fig. 6, one can clearly see that the MnO<sub>x</sub> promotion strongly depends on gas phase O2 concentration. When sufficient gas phase molecular O<sub>2</sub> is present, the MnO<sub>x</sub> promotion effect is low. In contrast, the MnO<sub>x</sub> promotion gradually becomes significant with a decrease in gas phase molecular O2 concentration (or higher O2 conversion), suggesting that the MnO<sub>x</sub> sites play a mediator role for oxygen exchange between the gas phase and catalyst lattice. To further elaborate on this, the oxygen exchange happens in both ways: (i) the gas phase O2 is supplied to the reduced catalytic oxide phase by the MnO<sub>x</sub> center. This is evident by the cyclic H2-TPR experiment (see Fig. 4) where the supported 5Na<sub>2</sub>WO<sub>4</sub>/SiO<sub>2</sub> catalyst regains almost all lattice oxygen species during the reoxidation step only in the presence of  $MnO_x$  species. (ii) Catalytic oxygen is supplied to the catalyst surface for consumption. Thus, the presence of MnO<sub>x</sub> species increases the total amount of oxygen release that results in significant improvement in catalytic performance (activity as well as selectivity) [15,35].

The current conclusions are in agreement with many literature reports claiming that  $\rm MnO_x$  participates in oxygen spillover to the W-oxide centers. [3,17,19–23] Recent *in-situ/operando* XRD and Raman studies reported that the oxygen exchange between gas phase and catalyst oxide lattice takes place *via* the reversible cycle of  $\rm Mn_7SiO_{12} \leftrightarrow MnWO_4$ . [13] Other *ex-situ* studies speculated the  $\rm Mn_2O_3 \leftrightarrow MnWO_4$  redox cycle to be operational for oxygen exchange. [51,52] Such 3D oxide phases, however, were not detected in the current study with the supported 1.2Mn-5Na<sub>2</sub>WO<sub>4</sub>/SiO<sub>2</sub> catalyst during OCM. It is, thus, proposed that the thermally and chemically stable surface  $\rm MnO_x$  sites in the current 1.2Mn-5Na<sub>2</sub>WO<sub>4</sub>/SiO<sub>2</sub> catalyst are responsible for facilitating oxygen exchange between gas-phase molecular O<sub>2</sub> and the W-oxide phases.

### 4.7. Influence of temperature on $MnO_x$ promotion

At similar oxygen conversion, the promotional effect of  $MnO_x$  on  $CH_4$  activity was found to be higher at lower reaction temperatures (see Fig. 6(a) and (c)). This observation is in agreement with literature reports that observed  $MnO_x$  promotion allows the catalyst to conduct the OCM reaction at a much lower reaction temperature than for the unpromoted, supported  $5Na_2WO_4/SiO_2$  catalyst. [29] However, the  $CH_4$  can be activated by both the surface  $Na-WO_x$  sites and molten  $Na_2WO_4$  phase. [15] For the supported  $5Na_2WO_4/SiO_2$  catalyst, the  $C_2$  and  $CO_2$  (primarily formed by surface  $Na-WO_x$  species), and  $CO_2$  (mostly coming from the molten  $Na_2WO_4$  phase) [15] selectivity values do not change significantly with increasing reaction temperature (see Fig. 7). This suggests the activity of both of these sites increase proportionately with temperature, in the absence of  $MnO_x$  species. In contrast, for the



Scheme 1. OCM reaction mechanism over supported Mn-Na<sub>2</sub>WO<sub>4</sub>/SiO<sub>2</sub> catalysts.

supported 1.2Mn-5Na $_2$ WO $_4$ /SiO $_2$  catalyst, the C $_2$  and CO selectivity increase, and CO $_2$  selectivity decreases with temperature. Such an interesting change in the selectivity of C $_2$  and CO (increasing with temperature) and CO $_2$  (decreasing with temperature) is also reported in the OCM literature for 1.2Mn-5Na $_2$ WO $_4$ /SiO $_2$  catalyst, both at atmospheric and elevated pressures (0.2–0.4 MPa). [46,53] These observations suggest that MnO $_x$  selectively promotes the molten Na $_2$ WO $_4$  phase at lower temperature and that the MnO $_x$  promotion of surface Na-WO $_x$  sites becomes dominant at higher temperatures.

### 5. Conclusions

The structural dynamics of the supported  $1.2Mn-5Na_2WO_4/SiO_2$  catalyst under OCM reaction conditions were investigated with multiple in-situ characterization techniques and chemical probe measurements. The role and promotional effect of  $MnO_x$  phase was investigated via controlled TAP experiments and detailed steady state kinetic studies. The findings are summarized as follows:

- (i) The freshly calcined, dehydrated 1.2Mn-5Na $_2$ WO $_4$ /SiO $_2$  catalyst contains (at 400 °C, oxidizing environment) crystalline Mn $_2$ O $_3$ , Na $_2$ WO $_4$  and  $\beta$ -cristobalite (SiO $_2$ ) phases along with surface MnO $_x$  and Na-WO $_x$  sites. Heating the catalyst to 900 °C (oxidizing environment) results in melting of the crystalline Na $_2$ WO $_4$  phase. Interestingly, the WO $_4$  structure originally present in Na $_2$ WO $_4$  crystal is preserved in its molten phase.
- (ii) In the OCM reaction environment at 900 °C, the  $Mn_2O_3$  crystalline phase disappears, possibly due to the reduction of Mn-oxide. In contrast, the surface  $MnO_x$  and  $Na\text{-}WO_x$  sites exhibit excellent thermal and chemical stability and  $Na_2WO_4$  remains in molten phase.
- (iii) Deeper analysis of the *in-situ* Raman spectra provided the first ever direct spectroscopic evidence regarding the interaction between Mn and W-oxide (molten Na<sub>2</sub>WO<sub>4</sub> phase and surface Na-WO<sub>x</sub> sites) centers. Further analysis revealed that the treatment of the supported 1.2Mn-5Na<sub>2</sub>WO<sub>4</sub>/SiO<sub>2</sub> catalyst in the OCM reaction environment results in formation of new surface Na-WO<sub>x</sub> sites from redispersion of molten Na<sub>2</sub>WO<sub>4</sub> phase on the SiO<sub>2</sub> support [15].
- (iv) The  $MnO_x$  species are active towards  $CH_4$  conversion, but not selective. The addition of  $MnO_x$  to the supported  $5Na_2WO_4/SiO_2$  catalysts, however, significantly improves the catalyst activity without affecting the  $C_2$  selectivity. This suggests that the Woxide centers are the catalytic active site for OCM and that the

- $MnO_x$  species *only* act as promoters in the supported 1.2Mn- $5Na_2WO_4/SiO_2$  catalyst.
- (v) The promotional effect of  $MnO_x$  is strongly dependent on the reaction conditions. At low availability of gas-phase molecular  $O_2$ , the promotional effect becomes significant suggesting  $MnO_x$  species act as mediators for oxygen exchange between the gas phase and catalyst lattice.
- (vi) MnO<sub>x</sub> promotion of the catalytically active molten Na<sub>2</sub>WO<sub>4</sub> phase and surface Na-WO<sub>x</sub> sites varies as a function of reaction temperature. At low temperature, the MnO<sub>x</sub> species selectively promote the molten Na<sub>2</sub>WO<sub>4</sub> phase and at high temperature the MnO<sub>x</sub> promotion of the surface Na-WO<sub>x</sub> sites becomes dominant.

These new findings add clarity to the debates in the literature regarding stable structures, role, and promotional effect of  $MnO_x$  in the supported  $Mn\textsubscript{NnO}_x/SiO_2$  catalyst during the OCM reaction. Based on the new findings from this study, along with the findings from the published articles [15,35], we propose the OCM reaction mechanism to take place over supported  $Mn\textsubscript{NnO}_x/SiO_2$  catalysts as presented in Scheme 1.

### CRediT authorship contribution statement

Sagar Sourav: Conceptualization, Methodology, Validation, Investigation, Writing – original draft. Daniyal Kiani: Conceptualization, Methodology, Writing – review & editing. Yixiao Wang: Conceptualization, Methodology, Validation, Writing – review & editing, Supervision. Jonas Baltrusaitis: Conceptualization, Methodology, Writing – review & editing, Supervision, Funding acquisition. Rebecca R. Fushimi: Conceptualization, Methodology, Writing – review & editing, Supervision, Funding acquisition. Israel E. Wachs: Conceptualization, Methodology, Writing – review & editing, Supervision, Funding acquisition.

### **Declaration of Competing Interest**

The authors declare that they have no known competing financial interests or personal relationships that could have appeared to influence the work reported in this paper.

### **Data Availability**

The data set generated during the current study are available from the corresponding authors upon reasonable request.

#### Acknowledgements

DK, JB and IEW gratefully acknowledge the National Science Foundation (NSF) Chemical, Bioengineering, Environment and Transport Systems (CBET) award # 1706581. SS, YW and RRF gratefully acknowledge the support from the U.S. Department of Energy (USDOE), Office of Energy Efficiency and Renewable Energy (EERE), Advanced Manufacturing Office Next Generation R&D Projects under contract no. DE-AC07-05ID14517. All the authors acknowledge the assistance from Dr. Henry Luftman of Lehigh University for conducting NAP-XPS experiments and Arnold W. Erickson of Idaho National Laboratory for collecting the in-situ XRD spectra. SS, DK, JB and IEW also sincerely thank Dr. Michael E. Ford of the Operando Molecular Spectroscopy & Catalysis Research Laboratory, Lehigh University, for his insightful input. SS, YW and RRF sincerely thank James P. Pittman of Idaho National Laboratory for his help in the lab in preparing isotope gas mixtures, setting up the steady state fixed-bed reactor and maintaining the TAP reactor.

### Appendix A. Supporting information

Supplementary data associated with this article can be found in the online version at doi:10.1016/j.cattod.2022.07.005.

#### References

- J. Lin, J. Gu, D. Yang, C. Zhang, Stability Test of W-Mn/SiO<sub>2</sub> catalyst for oxidative coupling of methane, Petrochem. Technol. 24 (1995), 293-293.
- [2] X. Wang, J. Zhang, D. Yang, C. Zhang, J. Lin, S. Li, Oxiditive coupling of methane over W-Mn/SiO<sub>2</sub> catalyst in a bench-scale stainless steel fluidized-bed, React. Petrochem. Technol. 26 (1997) 361–367.
- [3] S.B. Li, Oxidative coupling of methane over W-Mn/SiO<sub>2</sub> catalyst, Chin. J. Chem. 19 (1) (2001) 16–21.
- [4] S.B. Li, Reaction chemistry of W-Mn/SiO<sub>2</sub> catalyst for the oxidative coupling of methane, J. Nat. Gas. Chem. 12 (1) (2003) 1–9.
- [5] S. Arndt, T. Otremba, U. Simon, M. Yildiz, H. Schubert, R. Schomäcker, Mn–Na<sub>2</sub>WO<sub>4</sub>/SiO<sub>2</sub> as catalyst for the oxidative coupling of methane. What is really known? Appl. Catal., A 425–426 (2012) 53–61.
- [6] D. Kiani, S. Sourav, J. Baltrusaitis, I.E. Wachs, Oxidative coupling of methane (OCM) by SiO<sub>2</sub>-supported tungsten oxide catalysts promoted with Mn and Na, ACS Catal. 9 (7) (2019) 5912–5928.
- [7] S. Hou, Y. Cao, W. Xiong, H. Liu, Y. Kou, Site requirements for the oxidative coupling of methane on SiO<sub>2</sub>-supported Mn catalysts, Ind. Eng. Chem. Res. 45 (21) (2006) 7077–7083
- [8] A. Vamvakeros, S. Jacques, V. Middelkoop, M. Di Michiel, C. Egan, I. Ismagilov, G. Vaughan, F. Gallucci, M. van Sint Annaland, P. Shearing, Real time chemical imaging of a working catalytic membrane reactor during oxidative coupling of methane, Chem. Commun. 51 (64) (2015) 12752–12755.
- [9] M. Yildiz, Y. Aksu, U. Simon, T. Otremba, K. Kailasam, C. Göbel, F. Girgsdies, O. Görke, F. Rosowski, A. Thomas, R. Schomäcker, S. Arndt, Silica material variation for the Mn<sub>x</sub>O<sub>y</sub>-Na<sub>2</sub>WO<sub>4</sub>/SiO<sub>2</sub>, Appl. Catal. A 525 (2016) 168–179.
- [10] D. Matras, A. Vamvakeros, S. Jacques, N. Grosjean, B. Rollins, S. Poulston, G.B. G. Stenning, H. Godini, J. Drnec, R.J. Cernik, A.M. Beale, Effect of thermal treatment on the stability of Na-Mn-W/SiO<sub>2</sub> catalyst for the oxidative coupling of methane, Faraday Discuss. 229 (2021) 176–196.
- [11] A. Vamvakeros, D. Matras, S.D.M. Jacques, M. di Michiel, S.W.T. Price, P. Senecal, M.A. Aran, V. Middelkoop, G.B.G. Stenning, J.F.W. Mosselmans, I.Z. Ismagilov, A. M. Beale, Real-time multi-length scale chemical tomography of fixed bed reactors during the oxidative coupling of methane reaction, J. Catal. 386 (2020) 39–52.
- [12] D. Kiani, S. Sourav, I.E. Wachs, J. Baltrusaitis, Synthesis and molecular structure of model silica-supported tungsten oxide catalysts for oxidative coupling of methane (OCM), Catal. Sci. Technol. 10 (2020) 3334–3345.
- [13] M.J. Werny, Y. Wang, F. Girgsdies, R. Schlögl, A. Trunschke, Fluctuating Storage of the Active Phase in a Mn-Na<sub>2</sub>WO<sub>4</sub>/SiO<sub>2</sub> Catalyst for the Oxidative Coupling of Methane. Angew. Chem, Int. Ed. 59 (35) (2020) 14921–14926.
- [14] D. Kiani, S. Sourav, J. Baltrusaitis, I.E. Wachs, Elucidating the effects of Mn promotion on SiO<sub>2</sub>-supported Na-promoted tungsten oxide catalysts for oxidative coupling of methane (OCM), ACS Catal. 11 (2021) 10131–10137.
- [15] S. Sourav, Y. Wang, D. Kiani, J. Baltrusaitis, R.R. Fushimi, I.E. Wachs, New mechanistic and reaction pathway insights for oxidative coupling of methane (OCM) over supported Na<sub>2</sub>WO<sub>4</sub>/SiO<sub>2</sub>, Catal. Angew. Chem., Int. Ed. 60 (39) (2021) 21502–21511.
- [16] C.A. Ortiz-Bravo, S.J.A. Figueroa, R. Portela, C.A. Chagas, M.A. Bañares, F. S. Toniolo, Elucidating the structure of the W and Mn sites on the Mn-Na<sub>2</sub>WO<sub>4</sub>/SiO<sub>2</sub> catalyst for the oxidative coupling of methane (OCM) at real reaction temperatures. J. Catal. (2021).
- [17] Z. Aydin, A. Zanina, V.A. Kondratenko, J. Rabeah, J. Li, J. Chen, Y. Li, G. Jiang, H. Lund, S. Bartling, D. Linke, E.V. Kondratenko, Effects of N<sub>2</sub>O and water on

- activity and selectivity in the oxidative coupling of methane over Mn-Na<sub>2</sub>WO<sub>4</sub>/SiO<sub>2</sub>: role of oxygen species, ACS Catal. 12 (2) (2022) 1298-1309.
- [18] K. Takanabe, A.M. Khan, Y. Tang, L. Nguyen, A. Ziani, B.W. Jacobs, A.M. Elbaz, S. M. Sarathy, F. Tao, Integrated in situ characterization of a molten salt catalyst surface: evidence of sodium peroxide and hydroxyl radical formation, Angew. Chem. Int. Ed. 56 (35) (2017) 10403–10407.
- [19] Z.C. Jiang, C.J. Yu, X.P. Fang, S.B. Li, H.L. Wang, Oxide/support interaction and surface reconstruction in the Na<sub>2</sub>WO<sub>4</sub>/SiO<sub>2</sub> system, J. Phys. Chem. 97 (49) (1993) 12870–12875
- [20] J. Wu, S. Li, The role of distorted WO<sub>4</sub> in the oxidative coupling of methane on supported tungsten oxide catalysts, J. Phys. Chem. 99 (13) (1995) 4566–4568.
- [21] J. Wu, S. Li, J. Niu, X. Fang, Mechanistic study of oxidative coupling of methane over Mn2O3 Na2WO4SiO2 catalyst, Appl. Catal. A: Gen. 124 (1) (1995) 9–18.
- [22] H.S. Chen, J.Z.N. Zhang B., S.B. Li, Acta Phys. Chim. Sin. 17 (2001) 111-115.
- [23] S. Li, Reaction chemistry of W-Mn/SiO~ 2 catalyst for the oxidative coupling of methane, J. Nat. Gas. Chem. 12 (1) (2003) 1–9.
- [24] Y. Kou, B. Zhang, J.Z. Niu, S.B. Li, H.L. Wang, T. Tanaka, S. Yoshida, Amorphous features of working catalysts: XAFS and XPS characterization of Mn/Na<sub>2</sub>WO<sub>4</sub>/SiO<sub>2</sub> as used for the oxidative coupling of methane, J. Catal. 173 (2) (1998) 399–408.
- [25] D.J. Wang, M.P. Rosynek, J.H. Lunsford, Oxidative coupling of methane over oxide-supported sodium-manganese catalysts, J. Catal. 155 (2) (1995) 390–402.
- [26] S.F. Ji, T.C. Xiao, S.B. Li, C.Z. Xu, R.L. Hou, K.S. Coleman, M.L.H. Green, The relationship between the structure and the performance of Na-W-Mn/SiO<sub>2</sub> catalysts for the oxidative coupling of methane, Appl. Catal., A 225 (1) (2002) 271–284.
- [27] T.W. Elkins, H.E. Hagelin-Weaver, Characterization of Mn-Na<sub>2</sub>WO<sub>4</sub>/SiO<sub>2</sub> and Mn-Na<sub>2</sub>WO<sub>4</sub>/MgO catalysts for the oxidative coupling of methane, Appl. Catal., A 497 (2015) 96–106.
- [28] A. Shubin, I. Zilberberg, I. Ismagilov, E. Matus, M. Kerzhentsev, Z. Ismagilov, Hydrogen abstraction from methane on cristobalite supported W and Mn oxo complexes: a DFT study, Mol. Catal. 445 (2018) 307–315.
- [29] A. Malekzadeh, M. Abedini, A.A. Khodadadi, M. Amini, H.K. Mishra, A.K. Dalai, Critical influence of Mn on low-temperature catalytic activity of Mn/Na<sub>2</sub>WO<sub>4</sub>/SiO<sub>2</sub> catalyst for oxidative coupling of methane, Catal. Lett. 84 (1) (2002) 45–51.
- [30] B. Beck, V. Fleischer, S. Arndt, M.G. Hevia, A. Urakawa, P. Hugo, R. Schomäcker, Oxidative coupling of methane-a complex surface/gas phase mechanism with strong impact on the reaction engineering, Catal. Today 228 (2014) 212–218.
- [31] V. Fleischer, R. Steuer, S. Parishan, R. Schomäcker, Investigation of the surface reaction network of the oxidative coupling of methane over Na<sub>2</sub>WO<sub>4</sub>/Mn/SiO<sub>2</sub> catalyst by temperature programmed and dynamic experiments, J. Catal. 341 (2016) 91–103.
- [32] Y. Gordienko, T. Usmanov, V. Bychkov, V. Lomonosov, Z. Fattakhova, Y. Tulenin, D. Shashkin, M. Sinev, Oxygen availability and catalytic performance of NaWMn/ SiO<sub>2</sub> mixed oxide and its components in oxidative coupling of methane, Catal. Today 278 (2016) 127–134.
- [33] V.I. Lomonosov, Y.A. Gordienko, M.Y. Sinev, V.A. Rogov, V.A. Sadykov, Thermochemical properties of the lattice oxygen in W, Mn-containing mixed oxide catalysts for the oxidative coupling of methane, Russ. J. Phys. Chem. A 92 (3) (2018) 430–437
- [34] Z. Aydin, V.A. Kondratenko, H. Lund, S. Bartling, C.R. Kreyenschulte, D. Linke, E. V. Kondratenko, Revisiting activity- and selectivity-enhancing effects of water in the oxidative coupling of methane over MnO<sub>x</sub>-Na<sub>2</sub>WO<sub>4</sub>/SiO<sub>2</sub> and proving for other materials, ACS Catal. 10 (15) (2020) 8751–8764.
- [35] S. Sourav, Y. Wang, D. Kiani, J. Baltrusaitis, R.R. Fushimi, I.E. Wachs, Resolving the Types and Origin of Lattice Oxygen Species Present in Supported Mn-Na<sub>2</sub>WO<sub>4</sub>/ SiO<sub>2</sub> Catalysts for Oxidative Coupling of Methane, ACS Catal. 11 (2021) 10288–10293.
- [36] S. Sourav, I.E. Wachs, Cr-Free, Cu promoted Fe oxide-based catalysts for high-temperature water-gas shift (HT-WGS) reaction, Catalysts 10 (2020) 3.
- [37] V. Fleischer, U. Simon, S. Parishan, M.G. Colmenares, O. Görke, A. Gurlo, W. Riedel, L. Thum, J. Schmidt, T. Risse, K.-P. Dinse, R. Schomäcker, Investigation of the role of the Na<sub>2</sub>WO<sub>4</sub>/Mn/SiO<sub>2</sub> catalyst composition in the oxidative coupling of methane by chemical looping experiments, J. Catal. 360 (2018) 102–117.
- [38] E.I. Ross-Medgaarden, I.E. Wachs, Structural determination of bulk and surface tungsten oxides with UV-vis diffuse reflectance spectroscopy and raman spectroscopy, J. Phys. Chem. C. 111 (41) (2007) 15089–15099.
- [39] C.M. Julien, M. Massot, C. Poinsignon, Lattice vibrations of manganese oxides: Part I. Periodic structures, Spectrochim. Acta Part A: Mol. Biomol. Spectrosc. 60 (3) (2004) 689–700.
- [40] Y.F. Han, K. Ramesh, L. Chen, E. Widjaja, S. Chilukoti, F. Chen, Observation of the reversible phase-transformation of α-Mn2O3 nanocrystals during the catalytic combustion of methane by in situ raman spectroscopy, J. Phys. Chem. C. 111 (7) (2007) 2830–2833.
- [41] D. Kiani, S. Sourav, W. Taifan, M. Calatayud, F. Tielens, I.E. Wachs, J. Baltrusaitis, Existence and properties of isolated catalytic sites on the surface of β-cristobalite-supported, doped tungsten oxide catalysts (WO<sub>x</sub>/β-SiO<sub>2</sub>, Na-WO<sub>x</sub>/β-SiO<sub>2</sub>, Mn-WO<sub>x</sub>/β-SiO<sub>2</sub>) for oxidative coupling of methane (OCM): a combined periodic DFT and experimental study, ACS Catal. 10 (2020) 4580–4592.
- [42] M.N. Iliev, M.M. Gospodinov, A.P. Litvinchuk, Raman spectroscopy of MnWO<sub>4</sub>, Phys. Rev. B 80 (21) (2009), 212302.
- [43] S. Lwin, Y. Li, A.I. Frenkel, I.E. Wachs, Nature of WO<sub>x</sub> Sites on SiO<sub>2</sub> and their molecular structure–reactivity/selectivity relationships for propylene metathesis, ACS Catal. 6 (5) (2016) 3061–3071.
- [44] F. Buciuman, F. Patcas, R. Craciun, R.T. Zahn, D, Vibrational spectroscopy of bulk and supported manganese oxides, Phys. Chem. Chem. Phys. 1 (1) (1999) 185–190.
- [45] J. Wang, J. You, M. Wang, L. Lu, A.A. Sobol, S. Wan, In-situ high-temperature Raman spectroscopic studies of the vibrational characteristics and microstructure

### ARTICLE IN PRESS

S. Sourav et al. Catalysis Today xxx (xxxx) xxx

- evolution of sodium tungstate dihydrate crystal during heating and melting, J. Raman Spectrosc. 49 (10) (2018) 1693–1705.
- [46] S.M.K. Shahri, A.N. Pour, Ce-promoted Mn/Na2WO4/SiO2 catalyst for oxidative coupling of methane at atmospheric pressure, J. Nat. Gas. Chem. 19 (1) (2010) 47–53
- [47] S.M.K. Shahri, S.M. Alavi, Kinetic studies of the oxidative coupling of methane over the Mn/Na<sub>2</sub>WO<sub>4</sub>/SiO<sub>2</sub> catalyst, J. Nat. Gas. Chem. 18 (1) (2009) 25–34.
- [48] J. Si, G. Zhao, W. Sun, J. Liu, C. Guan, Y. Yang, X.-R. Shi, Y. Lu, Oxidative coupling of methane: examining the inactivity of the MnO<sub>x</sub>-Na<sub>2</sub>WO<sub>4</sub>/SiO<sub>2</sub> catalyst at low temperature, Angew. Chem. Int. Ed. (2022), e202117201.
- [49] D. Kiani, S. Sourav, I.E. Wachs, J. Baltrusaitis, A combined computational and experimental study of methane activation during oxidative coupling of methane (OCM) by surface metal oxide catalysts, Chem. Sci. 12 (42) (2021) 14143–14158.
- [50] B. Huang, N.S. Hayek, G. Sun, S. Mottaghi-Tabar, D.S.A. Simakov, O.M. Gazit, Correlating properties of the Mn<sub>2</sub>O<sub>3</sub>-Na<sub>2</sub>WO<sub>4</sub>/SiO<sub>2</sub> catalyst with statistically estimated parameters for the oxidative coupling of methane, Energy Fuels 35 (11) (2021) 9589–9598.
- [51] J. Wu, S. Li, J. Niu, X. Fang, Mechanistic study of oxidative coupling of methane over Mn<sub>2</sub>O<sub>3</sub>-Na<sub>2</sub>WO<sub>4</sub>/SiO<sub>2</sub> catalyst, Appl. Catal., A 124 (1) (1995) 9–18.
- [52] P. Wang, G. Zhao, Y. Wang, Y. Lu, MnTiO<sub>3</sub>-driven low-temperature oxidative coupling of methane over TiO<sub>2</sub>-doped Mn<sub>2</sub>O<sub>3</sub>-Na<sub>2</sub>WO<sub>4</sub>/SiO<sub>2</sub> catalyst, Sci. Adv. 3 (6) (2017), e1603180.
- [53] J.S. Ahari, M.T. Sadeghi, S. Zarrinpashne, Effects of operating parameters on oxidative coupling of methane over Na-W-Mn/SiO<sub>2</sub> catalyst at elevated pressures, J. Nat. Gas. Chem. 20 (2) (2011) 204–213.